Ensemble Kalman Filter Assimilation of HIWRAP Observations of Hurricane Karl (2010) from the Unmanned Global Hawk Aircraft

JASON A. SIPPEL

Laboratory for Atmospheres, NASA Goddard Space Flight Center, Greenbelt, and Goddard Earth Sciences Technology and Research, Morgan State University, Baltimore, Maryland

FUQING ZHANG AND YONGHUI WENG

Department of Meteorology, The Pennsylvania State University, University Park, Pennsylvania

LIN TIAN

Laboratory for Atmospheres, NASA Goddard Space Flight Center, Greenbelt, and Goddard Earth Sciences Technology and Research, Morgan State University, Baltimore, Maryland

GERALD M. HEYMSFIELD AND SCOTT A. BRAUN

Laboratory for Atmospheres, NASA Goddard Space Flight Center, Greenbelt, Maryland

(Manuscript received 23 January 2014, in final form 20 August 2014)

ABSTRACT

This study utilizes an ensemble Kalman filter (EnKF) to assess the impact of assimilating observations of Hurricane Karl from the High-Altitude Imaging Wind and Rain Airborne Profiler (HIWRAP). HIWRAP is a new Doppler radar on board the NASA Global Hawk unmanned airborne system, which has the benefit of a 24–26-h flight duration, or about 2–3 times that of a conventional aircraft. The first HIWRAP observations were taken during NASA's Genesis and Rapid Intensification Processes (GRIP) experiment in 2010. Observations considered here are Doppler velocity (Vr) and Doppler-derived velocity–azimuth display (VAD) wind profiles (VWPs). Karl is the only hurricane to date for which HIWRAP data are available. Assimilation of either Vr or VWPs has a significant positive impact on the EnKF analyses and forecasts of Hurricane Karl. Analyses are able to accurately estimate Karl's observed location, maximum intensity, size, precipitation distribution, and vertical structure. In addition, forecasts initialized from the EnKF analyses are much more accurate than a forecast without assimilation. The forecasts initialized from VWP-assimilating analyses perform slightly better than those initialized from Vr-assimilating analyses, and the latter are less accurate than EnKF-initialized forecasts from a recent proof-of-concept study with simulated data. Likely causes for this discrepancy include the quality and coverage of the HIWRAP data collected from Karl and the presence of model error in this real-data situation. The advantages of assimilating VWP data likely include the ability to simultaneously constrain both components of the horizontal wind and to circumvent reliance upon vertical velocity error covariance.

1. Introduction

This study examines the effectiveness of assimilating velocity data from the High-Altitude Imaging Wind and Rain Airborne Profiler (HIWRAP; Li et al. 2011) with an ensemble Kalman filter (EnKF). HIWRAP is a Doppler radar flown on the Global Hawk during the National Aeronautics and Space Administration's (NASA's) Genesis and Rapid Intensification Processes (GRIP) experiment (Braun et al. 2013) in 2010 and in NASA's Hurricane and Severe Storm Sentinel (HS3) experiment. The conically scanning radar uses two frequencies [Ka (35 GHz) and Ku (14 GHz)] and beams (30° and 40° incidence angles) and is designed for operation at high altitudes. The recent investigation by Sippel et al. (2013, hereafter S13) used simulated-data

Corresponding author address: Dr. Jason A. Sippel, NASA GSFC, Code 612, Greenbelt, MD 20771.
E-mail: jason.sippel@nasa.gov

DOI: 10.1175/MWR-D-14-00042.1

experiments to examine the potential usefulness of assimilating HIWRAP Doppler velocity (Vr), and the current study explores the assimilation of real HIWRAP observations taken from Hurricane Karl (2010). In particular, we compare the assimilation of quality-controlled Vr and velocity–azimuth display (VAD) wind profiles (VWPs). This is the first study to assimilate real HIWRAP observations.

A number of recent studies have shown that Vr can be useful for hurricane analyses with an EnKF, though the effectiveness of VWP assimilation has not yet been tested in this context. The results of S13 suggest that assimilating HIWRAP Vr can improve hurricane analyses and prediction, which is similar to findings of other studies (e.g., Zhao and Jin 2008; Zhang et al. 2009, 2011; Weng and Zhang 2012; Aksoy et al. 2012, 2013; Dong and Xue 2013) that have assimilated Vr within hurricanes with an EnKF. The results of Zhang et al. (2011) in particular demonstrate the systematic advantage of assimilating airborne Vr over a number of storms. After assimilating Vr observations from the National Oceanic and Atmospheric Administration (NOAA) WP-3D tail Doppler radar over a total of 61 missions from 14 tropical cyclones, they found a significant reduction in forecast track and intensity error relative to operational guidance.

Assimilation of VWP data offers a different approach to using Vr for hurricane analysis. The VAD method for estimating horizontal winds from Vr was developed by Lhermitte and Atlas (1961) and Browning and Wexler (1968) for ground-based radar and has recently been extended for application to HIWRAP by Tian et al. (2014, manuscript submitted to *J. Appl. Meteor. Climatol.*, hereafter T14). This method uses a sinusoidal fit to Vr distributed around a 360° circle to estimate the area-average nadir wind at a particular range. By repeating this process for different ranges, a nadir profile of VAD-estimated winds (i.e., a VWP) can be computed. HIWRAP's unique airborne scanning geometry lends itself to VWP computations, and this method cannot be used with the fore/aft scanning geometry of most other airborne radars. Though VWP data have not previously been assimilated for tropical cyclone analyses, a number of recent studies have used ground-based VWP retrievals for various other assimilation applications (e.g., Michelson and Seaman 2000; Benjamin et al. 2004, 2010; Zhu et al. 2013).

The motivation for testing HIWRAP VWP assimilation stems from HIWRAP's downward-pointing geometry. A concern, particularly for the inner beam, is the relatively large component tangent to the vertical axis. This is undesirable for data assimilation because of the potential for noisy or erroneous sample covariance associated with vertical velocity [see Fig. 17 of Poterjoy and Zhang (2011)]. In addition, the scans with steeper elevation angles observe a greater component of hydrometeor motion, which is an added source of error. This is much less of a problem for the NOAA WP-3D scanning geometry, which involves many near-horizontal measurements. By providing horizontal wind estimates, the VWP method can potentially circumvent these issues, though there are also sources of error in the assumptions used in calculating the VWP components. The two major assumptions most likely to introduce error are that winds vary linearly within the VWP footprint and that vertical velocity is constant along the edge of the footprint.

VWPs and Vr are fundamentally different, and it is up to this point unclear how these differences might impact analysis of a hurricane vortex. HIWRAP Vr is of very high resolution, and each observation represents the average radial wind over an approximately 2° × 2° × 150-m prism. Meanwhile, each VAD data point is an estimate of the horizontal wind components averaged over a circle whose area varies linearly with distance from the radar. Assuming an aircraft altitude of 20 km, the HIWRAP radar beams intersect the surface in concentric circles with radii of about 12 km (30° beam) and 17 km (40° beam).

Regardless of which HIWRAP velocity data are assimilated, using long-duration unmanned aircraft such as the Global Hawk is a potential solution to difficulties in gathering airborne radar data over hurricanes. Many tropical cyclones are too far out over the ocean to reach with current manned aircraft, and even when storms are within range, the typical on-station time for radar-bearing aircraft is less than 6 h. The Global Hawk is an ideal platform for observing tropical cyclones because of its long flight duration (up to 26 h), high altitude (>18 km), and ability to carry large payloads. If deployed from the eastern United States, the 20 000-km flight range allows the Global Hawk to be on station over storms for 10–14 h in the central Atlantic and 14–20 h in the western Atlantic (Braun et al. 2013).

The remainder of this study is organized as follows. Section 2 describes the storm to be studied and the methodology for the experiments. Section 3 examines EnKF analyses and subsequent EnKF-initialized forecasts, and section 4 follows with a discussion and the conclusions.

2. Background and methods

The experiments herein will focus on Hurricane Karl (2010), which was observed extensively during NASA's GRIP experiment (Braun et al. 2013). The pre-Karl depression formed from a westward-moving low pressure area in the central Caribbean, and the system

attained tropical storm strength north of Honduras late on 14 September. Karl intensified fairly quickly to near-hurricane intensity, making landfall on the Yucatan Peninsula shortly after 1200 UTC 15 September. The system weakened only slightly as it moved across the peninsula, and the inner core remained largely intact as it emerged over the Bay of Campeche early on 16 September [see Fig. 3a of Braun et al. (2013)]. Thereafter, the storm rapidly intensified to a hurricane by 1800 UTC 16 September and to a major hurricane by 1200 UTC 17 September. Karl moved westward across the Bay of Campeche and made landfall just before 1800 UTC north of Veracruz, Mexico.

a. *Data and quality control*

The Vr observations provided from the HIWRAP radar were collected during the Global Hawk flight on 16–17 September. The aircraft took off at 1200 UTC 16 September from Armstrong Flight Research Center at Edwards Air Force Base, California, and reached the outer bands of Karl between 1800 and 1900 UTC. The plane made 20 eye-crossing transects between 1900 UTC 16 September and 0800 UTC 17 September [e.g., Fig. 3b of Braun et al. (2013)].

Unfortunately, several problems were encountered with the HIWRAP data from Hurricane Karl since it was one of the radar's first flights on the Global Hawk. Foremost, only inner-beam (30° incidence) data are available from the flight. This represents a potentially significant disadvantage compared to the S13 simulated-data experiments, which assumed use of the outer beam (40° incidence). As mentioned in the introduction, this is undesirable for data assimilation because of the potential for noisy or erroneous sample covariance. Another problem encountered with this Vr data was a significant amount of noise (e.g., outliers) in the Doppler measurements that required strict quality control to correct (see below). This noise and other problems also contributed to inaccuracies in velocity unfolding for several legs that made measurements for those legs unusable. We want to emphasize that the details of noise removal and velocity and reflectivity thresholding detailed below are particular to data quality issues associated with the flight into Hurricane Karl. We anticipate less stringent quality-control requirements for future HIWRAP missions as a result of improvements in the data quality and availability of the outer beam.

Some quality-control steps were applied to both the Vr and VWP datasets. The initial step, including airplane velocity correction and Vr unfolding, was performed prior to data distribution. This dataset, along with a detailed description of the data processing, is available online at NASA's GRIP website (http://grip.nsstc.nasa.gov). Next, flight segments with faulty Vr unfolding were completely discarded since they could not be used. In addition, the results of T14 suggest that the best HIWRAP data from Karl are between roughly 2 and 8 km above sea level, so both Vr and VWP data above and below that layer are rejected.

For Vr assimilation, several additional procedures were also needed. First, an estimated fall speed was subtracted from Vr using a similar approach to that in Marks and Houze (1987). Precipitation below 5.0 km was assumed to be liquid while above 7.0 km it was assumed to be frozen. Between these two levels, we assumed a mixed-phase layer wherein the fall speed was determined from a weighted average (the weights vary linearly with height) of the frozen and liquid calculations. Furthermore, because much of the HIWRAP Vr from Karl is contaminated by significant amounts of noise, strict removal thresholds were required. In particular, any Vr data points greater than 40 m s^{-1} or less than 5 m s^{-1} were rejected, as were observations whose corresponding reflectivity was less than 25 dBZ (using a lower reflectivity threshold allows a considerable amount of noisy data to pass through). Comparing Figs. 1a and 1b reveals the impacts of these measures; Fig. 1a shows raw Vr, whereas Fig. 1b shows Vr with the quality-control measures described above.

After the initial quality control, a procedure similar to that in Zhang et al. (2009) was used to generate super observations (SOs). In particular, 15 consecutive volumes (~10 km along flight path) of quality-controlled Vr were binned to grids of 2 km in the radial direction and 20° in the azimuthal direction (see Fig. 2a; these respectively correspond to roughly 1.7- and 3 km vertical and horizontal distances). As in Zhang et al. (2009), volumes and bins with excessive variance were discarded, as were bins with fewer than 10 Vr observations. From each of these bins, the median Vr value was selected as the representative SO.

At this point, the average horizontal distance between Vr SOs was 5–6 km, though they needed to be thinned further because of a tendency for analyses to overfit the data. Thus, only 1/8 of the Vr SOs generated above were used for assimilation, and the average horizontal distance between SOs given to the EnKF system was about 16 km. To demonstrate the operation of the SO generation and thinning procedures, Figs. 1c,d illustrate example scatterplots of thinned and quality-controlled Vr SOs as a function of latitude and longitude. In Fig. 1c, SOs are generated from a single run (e.g., 15 volumes) of the procedure centered on the volume shown in Figs. 1a,b, and Fig. 1d shows similar data from the entire assimilation cycle at 0500 UTC 17 September (this was a center-crossing north–south transect). In general, between 100 and 250 Vr SOs were given to the assimilation system during each cycle (Fig. 2c), though there were a few cycles when little or no data were available. As a final level of quality control, any Vr SO whose

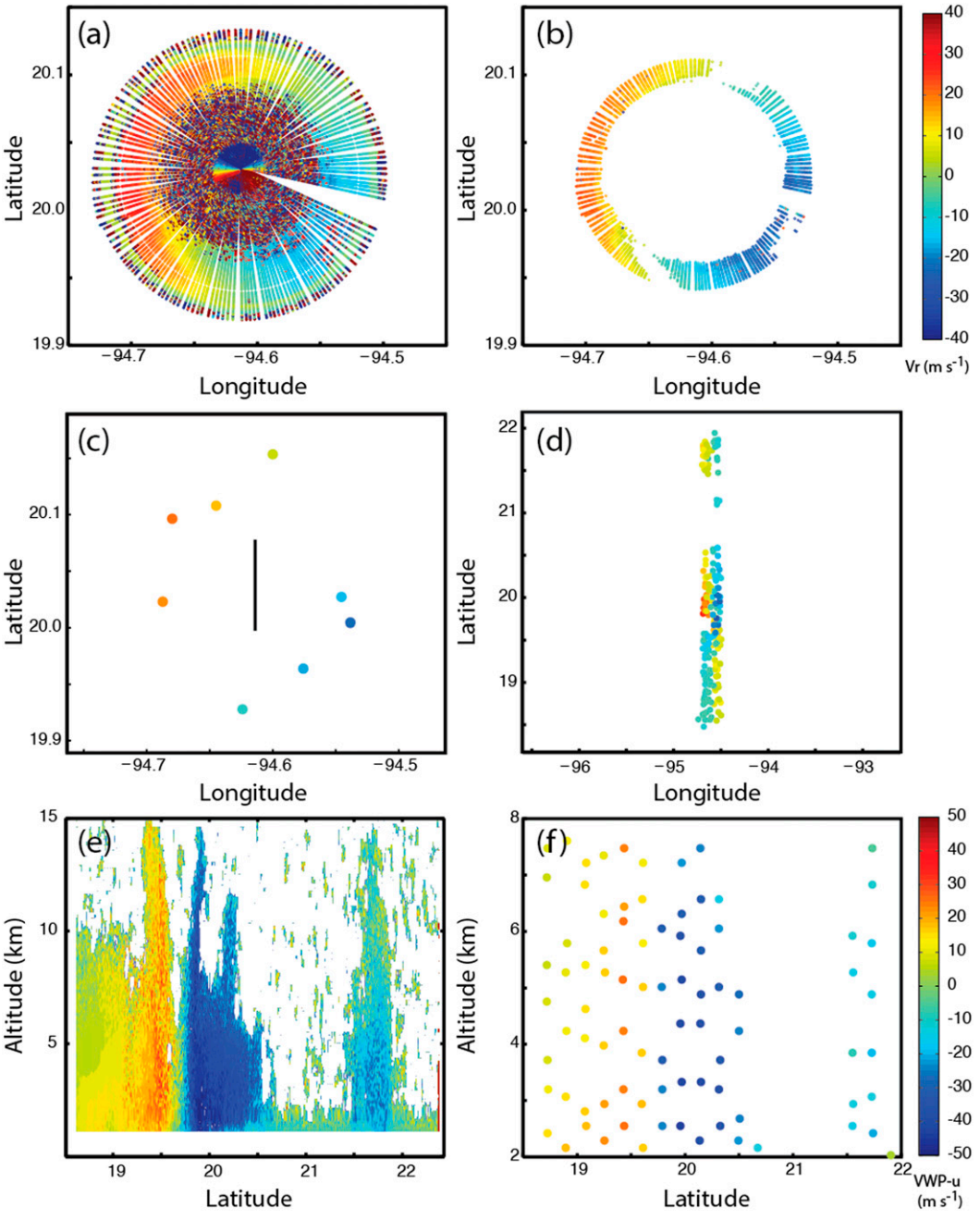

FIG. 1. Scatterplots of HIWRAP (a)–(d) Vr and (e)–(f) VWP observations of Hurricane Karl from the 0500 UTC 17 Sep cycle. In (a) a single unedited volume scan just north of Karl's eye is shown, while (b) shows the data that remain after removing all data below 2 km, above 8 km, and where the associated reflectivity is below 25 dBZ. In (c) a single run of the SO-generating procedure has been applied to the data in (b) in addition to the 14 surrounding volume scans (i.e., ~10 km of flight track, which is shown with a black line), and (d) shows all Vr SOs for the cycle. Note that the SOs in (c) and (d) span the 2–8-km layer. Finally, (e) shows raw VWP data covering the same region, and (f) shows resultant VWP SOs.

innovation exceeded 9 m s^{-1} was rejected, though the number of SOs rejected in this step was small (Fig. 2c).

The VWP data used here were produced from the algorithms employed in T14. To calculate VWP components, all Vr with returned power less than 10 dBZ were first eliminated, as were data where the aircraft pitch and roll exceeded 3°. In addition, VWP analyses were only performed for a particular range and 360° scan when postelimination data availability exceeded 50%, and noisy VWPs were eliminated based on

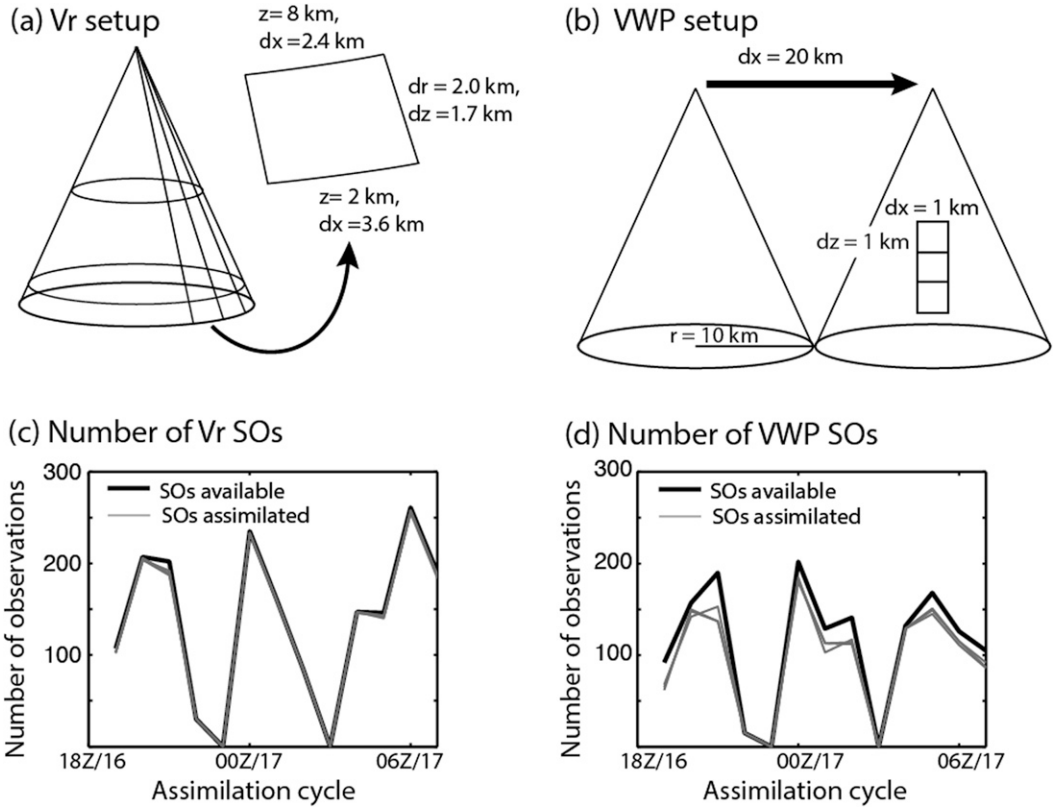

FIG. 2. (a),(b) Schematics demonstrating the SO binning strategy for Vr and VWP data and (c),(d) the number of SOs available and assimilated for each assimilation cycle. The multiple gray lines in (c),(d) represent the six experiments that assimilate HIWRAP data.

an areal standard deviation threshold described in T14. For the purpose of assimilation, VWP data with magnitudes less than $3\,\mathrm{m\,s^{-1}}$ or greater than $60\,\mathrm{m\,s^{-1}}$ were also rejected. Figure 1e shows the VWP u component for the same center-crossing overpass as above.

The differences between the Vr and VWP quality-control measures are driven mainly by the noisiness of Vr. Radial velocity data become noisy either in regions of high Doppler spectral width caused by high shear, low signal-to-noise ratio, and other factors, or when missing data packets result in errors in the Doppler calculation. In any of these cases, the uncertainty in the Doppler measurement will be significantly higher. For example, noisy Vr for reflectivities between 10 and 25 dBZ is not a major hindrance to VWP calculations in these regions. The same can be said for regions where the velocity magnitude was very low or high, and VWP thus can be used for a much greater range of velocities in Karl. One likely reason for the lower quality-control requirements for VWP than Vr is that each VWP data point is obtained from a sinusoidal fit to about 100–200 Vr observations distributed around a 360° circle, which tends to smooth the Doppler velocity fluctuations. A caveat of these differences is that data coverage between the Vr and VWP experiments can be different and thus comparison between the experiments is not always straightforward.

In addition to the Vr SO procedure discussed above, a rather simple VWP SO procedure has been developed in this study. Since the VWP product in essence represents the mean horizontal wind within the radar's footprint at a given range, it is important to ensure that footprints do not significantly overlap so that SOs contain independent information. To do this, each VWP u and v SO was assigned according to the median u and v values within bins that are approximately 20 km apart in the horizontal; there is no vertical separation between bins. As shown in Fig. 2b, 20 km is the minimum separation distance necessary to guarantee data independence assuming an aircraft altitude of 20 km and that data are only gathered down to the 2-km altitude. The size of each bin is about 1 km in both the horizontal and vertical directions, and the procedure requires at least five observations to produce an SO. The VWP u-component SOs generated by this procedure for the 0500 UTC assimilation cycle are shown in Fig. 1f, and Fig. 2d shows the total number of VWP SOs given to the

EnKF during each assimilation cycle. Finally, as with Vr, any VWP SO whose innovation exceeded 9 m s^{-1} was also rejected. Roughly 10% of VWP SOs are rejected in this step, though the number rejected is slightly different among the experiments (e.g., the multiple gray lines apparent in Fig. 2d).

b. *Model and assimilation setup*

The modeling and assimilation approaches here are similar to that in S13. Like S13, we use the Weather Research and Forecasting (WRF) Model (version 3.1.1) with two-way nesting to achieve 3-km grid spacing over the Bay of Campeche and surrounding terrain (see Fig. 1 of S13). All model domains have 35 vertical layers, and the model top is set at 10 hPa. Model physics choices include the Kain–Fritsch cumulus scheme (Kain and Fritsch 1990, 1993) on the 27- and 9-km grids, WRF single-moment 6-class microphysics with graupel (Hong et al. 2004), the Yonsei State University scheme (Noh et al. 2003) for planetary boundary layer (PBL) processes, and the Rapid Radiative Transfer Model longwave (Mlawer et al. 1997) and Dudhia shortwave (Dudhia 1989) radiation schemes. A set of 30 initial and boundary condition perturbations to the Global Forecast System (GFS) analysis and forecast initialized at 0000 UTC 16 September was used to create an ensemble of forecast realizations; this ensemble is termed no data assimilation (NODA) (NODA1-ENS from S13). Random large-scale differences from GFS were created by implanting balanced perturbations derived from National Centers for Environmental Prediction (NCEP) background error covariance statistics into the WRF variational data assimilation system (e.g., Barker et al. 2004).

c. *EnKF setup*

This study uses the regional-scale WRF-based EnKF system originally developed in Meng and Zhang (2008a,b). The system was later used to assimilate Doppler radar observations for convection-permitting hurricane analysis and forecasting in Zhang et al. (2009, 2011) and Weng and Zhang (2012). The EnKF setup in this study is similar to S13, but several additional procedures were used to improve results. First, the initial ensemble here was integrated for 12 h to develop background covariance, after which time the cyclone position was assimilated hourly until 1800 UTC[1] (see Fig. 3). The

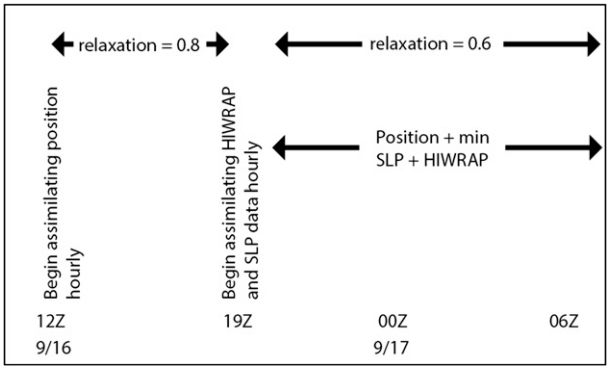

FIG. 3. Schematic illustrating the assimilation timeline.

position observations during this period were interpolated from National Hurricane Center best track data to the nearest tenth of a degree. At and after 1900 UTC, cyclone position, minimum sea level pressure, and HIWRAP data were all assimilated. The assimilation of position and minimum SLP (hereafter *P*/*I*) particularly helped to constrain the vortex during cycles when little or no HIWRAP data were available (see Figs. 2c,d). Cyclone center location during this time period was estimated from the HIWRAP data, again to the nearest tenth of a degree, and it was interpolated for cycles in which a center overpass was unavailable. Minimum SLP was interpolated from the best track data.[2]

The assumed uncertainty for *P*/*I* is consistent with Landsea and Franklin (2013) (i.e., 4 hPa for minimum SLP and 20 km for latitude and longitude), and several different observation uncertainty values are tested for VWP and Vr. The Vr measurement error from HIWRAP is roughly 1.5 m s^{-1} (Li et al. 2014, manuscript submitted to *IEEE Trans. Geosci. Remote Sens.*), and error due to fall speed estimation is roughly 1–2 m s^{-1} (Heymsfield et al. 2010). Thus, an appropriate error specification for Vr here is roughly 2–3 m s^{-1}, though we also test a value of 4 m s^{-1} because of the aforementioned data problems with Karl. Meanwhile, we were not able to determine an appropriate VWP error from peer-reviewed literature, so the 2–4 m s^{-1} values for Vr were also tested for VWP.

Covariance was localized using the Gaspari and Cohn (1999) fifth-order correlation function, and the radius of

[1] To find a center position, the assimilation routine searches for the minimum of a smoothed SLP field within 600 km of the observed center. If a value below 995 hPa is not found, then the routine searches for the maximum of the product of vertical vorticity and the fourth power of the surface pressure perturbation (i.e., 1030 − SLP). If intensity is assimilated, the minimum SLP is then defined to be the SLP at the center position.

[2] For real-time application, use of best track data would not be possible, and use of HIWRAP data for center location would be unlikely. Alternative sources in this circumstance include real-time advisories or NOAA P3 center fixes. However, since Karl was a mature and well-observed hurricane during this period, there is very little difference between the real-time, best track, and HIWRAP estimates.

TABLE 1. A description of the various assimilation experiments.

Expt	Detail	Assumed error ($m\,s^{-1}$) for Vr or VWP
NODA	Forecast from GFS initial conditions at 0000 UTC 16 Sep with no subsequent assimilation	—
CTRL	Assimilate position hourly from 1200 to 1800 UTC, then assimilate both position and minimum SLP	—
VR2	As in CTRL, but assimilate Vr hourly beginning at 1900 UTC	2
VR3	As in VR2, but change assumed Vr observation error	3
VR4	As in VR2, but change assumed Vr observation error	4
VWP2	As in CTRL, but assimilate VWP hourly beginning at 1900 UTC	2
VWP3	As in VWP2, but change assumed VWP observation error	3
VWP4	As in VWP2, but change assumed VWP observation error	4

influence (ROI) was different for the different observation types. Position and intensity data were assimilated at the lowest model level with an approximate 1200-km horizontal ROI and a 35-point vertical (i.e., distance in terms of model vertical levels[3]) ROI on all three domains. Meanwhile, the wind data were assimilated with the Z09 successive covariance localization (SCL) procedure, which uses a varying ROI, but we found that the ROI for the HIWRAP data needed to be adjusted downward by 25%. In particular, the EnKF assimilated 1/9 of the observations onto all domains with a horizontal ROI of 900 km. Meanwhile, an additional 2/9 of the observations were ingested into domains 2 and 3 with a horizontal ROI of 300 km, and the remaining 6/9 of the observations were assimilated on domain 3 with a 100-km horizontal ROI. Furthermore, the HIWRAP data are assimilated with a 26-point[4] vertical ROI. The percentage of observations assimilated into each domain is the same as in Weng and Zhang (2012) and Zhang et al. (2011).

To control filter divergence resulting from sampling and model error, the covariance relaxation of Zhang et al. [2004, their Eq. (5)] was used to inflate the covariance at updated grid points via a weighted average of the prior and posterior perturbations. All experiments here use a weight α that varies with time, starting out at 0.8 when only position is assimilated, and lowering to 0.6 when assimilation of minimum SLP and HIWRAP data commences. It was found that a static weight of 0.8 [e.g., that used in other hurricane studies such as Zhang et al. (2009, 2011); Weng and Zhang (2012)] resulted in unrealistically strong asymmetries in the wind field during later assimilation cycles, especially in the individual ensemble members. The purpose of the time-dependent relaxation is to maintain initially large mesoscale perturbations and to keep the later ensemble storm structures as realistic as possible (see Poterjoy et al. 2014).

The EnKF observation operator for Vr is based on linear interpolation of model fields, but that for VWP is slightly more complicated and accounts for the effective VWP averaging area. The Vr operator, which is the same as that utilized in S13, determines the position of forecast Vr values using the aircraft location in addition to the observation azimuth, elevation, and range. The forecast of Vr at a particular location is then calculated using linearly interpolated forecasts of horizontal and vertical velocity. This method does not account for beamwidth, though it is the same operator used successfully in Zhang et al. (2011) and the references therein. Meanwhile, forecasts of VWP data were calculated using the nominal latitude, longitude, altitude, incidence angle, and distance from the radar. Using this information, the VWP operator calculates the average horizontal wind components within a radius determined by the incidence angle and the distance between the radar and VWP observation.

3. Results

To assess the benefit of assimilating HIWRAP data, several experiments are compared. A control experiment, CTRL, examines the impact of *P*/*I* assimilation without any of the HIWRAP data. Only storm position is assimilated through 1800 UTC 16 September, and both position and minimum SLP are assimilated thereafter. Meanwhile, experiments VR*x* and VWP*x*, respectively, assimilate Vr and VWP observations in addition to the *P*/*I* data with *x* denoting the assumed observation uncertainty. In some figures, experiments are compared with NODA experiments, which are a deterministic and ensemble forecast without data assimilation. See Table 1 for a list and description of the experiments.

To assess the analysis quality, analyses are compared to HIWRAP data in addition to a number of parameters available from the automated tropical cyclone forecast (ATCF) B-deck. The B-deck parameters include the

[3] In terms of physical distance, the model top is roughly 30 km.

[4] The 2–8-km layer spanned by HIWRAP assimilation corresponds to roughly model levels 10–19. Thus, HIWRAP observations can to some extent influence the entire vertical domain.

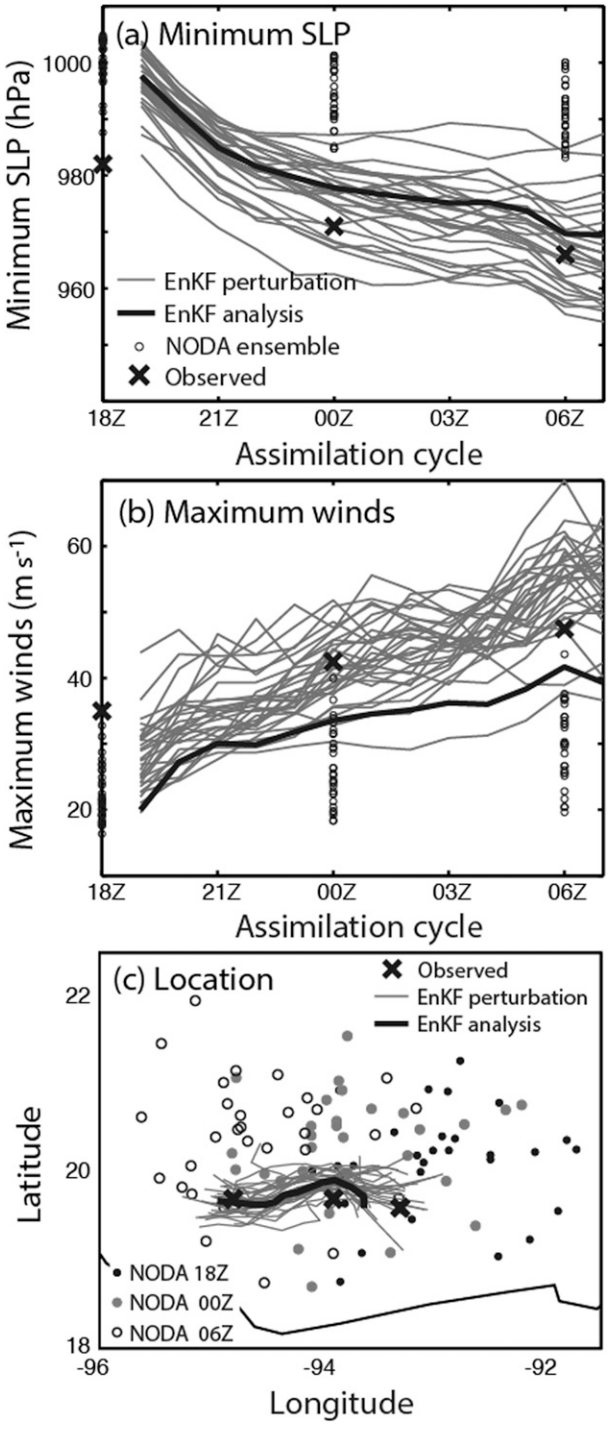

FIG. 4. The evolution of CTRL as compared with the best track data and the NODA ensemble in terms of (a) minimum SLP, (b) maximum winds, and (c) position. The best track location in (c) is shown at 1800 UTC 16 Sep and 0000 and 0600 UTC 17 Sep, and the coastline of Mexico is shown for reference.

maximum 10-m winds, minimum SLP, the radius of maximum winds (RMW), and radii of 64-kt (1 kt = 0.5144 m s^{-1}) winds (R64), 50-kt winds (R50), and 34-kt winds (R34) for each of the four quadrants relative to the storm center. The radius for each quadrant is defined to be the maximum extent of the particular wind strength in that quadrant. Instead of doing a quadrant-by-quadrant comparison for R64, R50, and R34, the average value is taken over all four quadrants as a proxy for the storm size. Meanwhile, track error was calculated using the location estimates described in section 2c, which implicitly relies upon the HIWRAP data.

In these comparisons, it is important to be aware of errors in the best track data. The recent work of Landsea and Franklin (2013) suggests that the average aircraft-observed category-2 or -3 hurricane has position uncertainty of roughly 20–30 km and intensity uncertainty of 4–5 m s^{-1} for maximum winds and 3–4 hPa for minimum SLP. The largest errors (as a percentage of the average parameter value, see their Table 2 and Fig. 7) are for wind radii; R34, R50, and R64 carry average uncertainties of 55, 45, and 30 km, respectively. For wind radii, this reflects error percentages of 25%–35%.

a. CTRL

The rather simple methodology of the CTRL analysis is successful at generating a hurricane vortex. Figure 4, which shows the time evolution of the CTRL analysis mean and perturbations along with the NODA ensemble, indicates that CTRL is much closer to the best track data than NODA. The NODA mean vortex (not shown) is very weak because of the storms in individual members all being quite weak (Figs. 4a,b) and spread over a large area (Fig. 4c). Meanwhile, the CTRL analysis is most successful in terms of the cyclone minimum SLP (Fig. 4a) and location (Figs. 4c and 5). The SLP error generally decreases with time (Fig. 4a) to about 3–4 hPa by the final analysis cycle. Figure 5 shows the evolution of position error, which also decreases with time in CTRL and stays roughly between 5 and 15 km during the latter half of the analysis period. Though the error in maximum winds also decreases with time (Fig. 4b), analysis maximum winds are still 7–8 m s^{-1} too weak even by the last few cycles. This is partly a result of the position spread in CTRL, which reduces analysis peak winds compared to the individual members.[5]

[5] The ensemble distributions of minimum SLP and maximum wind are not necessarily expected to be centered upon the truth or posterior mean for Eulerian assimilation. This is particularly true for the noisier wind fields, where it is likely that most members have maxima that are greater than that in the posterior mean. See S13 for a more in-depth discussion.

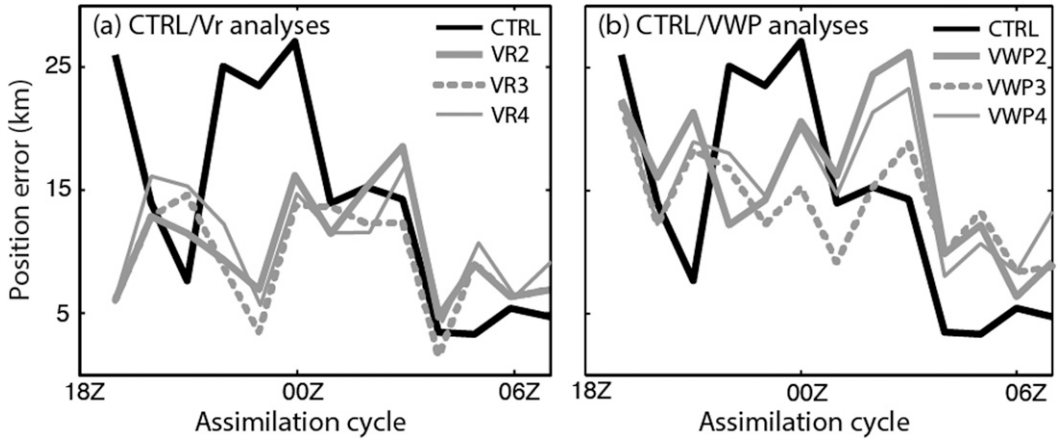

FIG. 5. The analysis error in storm center location as a function of analysis cycle for (a) Vr and (b) VWP experiments in addition to CTRL.

Despite this success, there are several problems with CTRL. One significant problem is that the CTRL analysis storm is much too large. To demonstrate this fact, Fig. 6 shows the evolution during the analysis period of the RMW and wind radii for the thresholds defined in the ATCF B-deck. The CTRL wind radii generally exceed the best track estimate by at least 25% and by more than 100% for the higher wind speeds. In addition, the CTRL storm also decays too rapidly with height, as suggested by the azimuthally averaged wind speeds as a function of radius and height at the final analysis cycle (Fig. 7). Though the azimuthal averages here are not directly comparable to the VWP retrievals, the upper-level wind speeds near the inner core in CTRL are far lower than those suggested in Fig. 1e. For example, Fig. 7 shows the 15 m s^{-1} contour in the eyewall extending up to 10–12 km, whereas the VWP data in the same region (Fig. 1e) suggest wind speeds were at least 25 m s^{-1} on both sides of the eyewall at this altitude. Furthermore, the vertical extent of strong winds and the rounded shape of the isopleths are inconsistent with expectations for a small, intense hurricane [e.g., Fig. 12 of Hawkins and Imbembo (1976)].

In terms of precipitation structure, there are both strengths and weaknesses in CTRL. To compare the observed and analyzed precipitation structures at 0700 UTC 17 September, Fig. 8 shows 0.5° reflectivity from the Alvarado, Mexico, radar[6] and CTRL analysis reflectivity at 3-km altitude. CTRL is fairly good at capturing the asymmetric distribution of precipitation, as the most intense precipitation is on the south and west sides of the analyzed and observed storms. However, the major weakness of CTRL is the lack of a compact, intense inner core. Whereas Karl had a well-defined and relatively small eyewall at the time, the comparable feature in CTRL is much larger and lacking in discrete structure. This result is consistent with the azimuthal wind field in Fig. 7.

b. Radial velocity assimilation

The results from the Vr-assimilating experiments indicate a substantial benefit from assimilating Vr in addition to *P*/*I*. The left columns of Figs. 9–10, which compare the evolution of maximum intensity in CTRL and the Vr-assimilating experiments, indicate that the addition of Vr helps bring analysis cyclone intensity closer to the best track estimates. On average the storms in the Vr analyses are 3–4 m s^{-1} stronger than CTRL in terms of maximum winds and about 6–7 hPa deeper in central pressure. Likewise, Figs. 5 and 11 show that the Vr-assimilating analysis storm locations are also generally closer to the observed location than in CTRL. In addition, Fig. 6 shows that storm size in these analyses is in much better agreement with the best track data. By the end of the assimilation period, the RMW in all three Vr experiments is commensurate with the observed RMW, which is about half that in CTRL (Fig. 6a). Though the radii for weaker winds are initially too large (Figs. 6c,e,g), they gradually decrease to very close to the best track estimates by the last few assimilation cycles. Furthermore, the strength of the mid- to upper-level wind speeds in the Vr-assimilating analyses (Fig. 12, left column) compares much more favorably with observations (Fig. 1e). Though again this is not a one-to-one comparison, there is much better agreement here than with CTRL. Likewise, the vertical structure of wind speeds is more consistent with that of a major hurricane (e.g., a taller and narrower circulation

[6] Note that the reflectivity values in Fig. 8a appear unrealistically low for a major hurricane. Thus, we only make qualitative comparisons between the observed and analyzed precipitation structures.

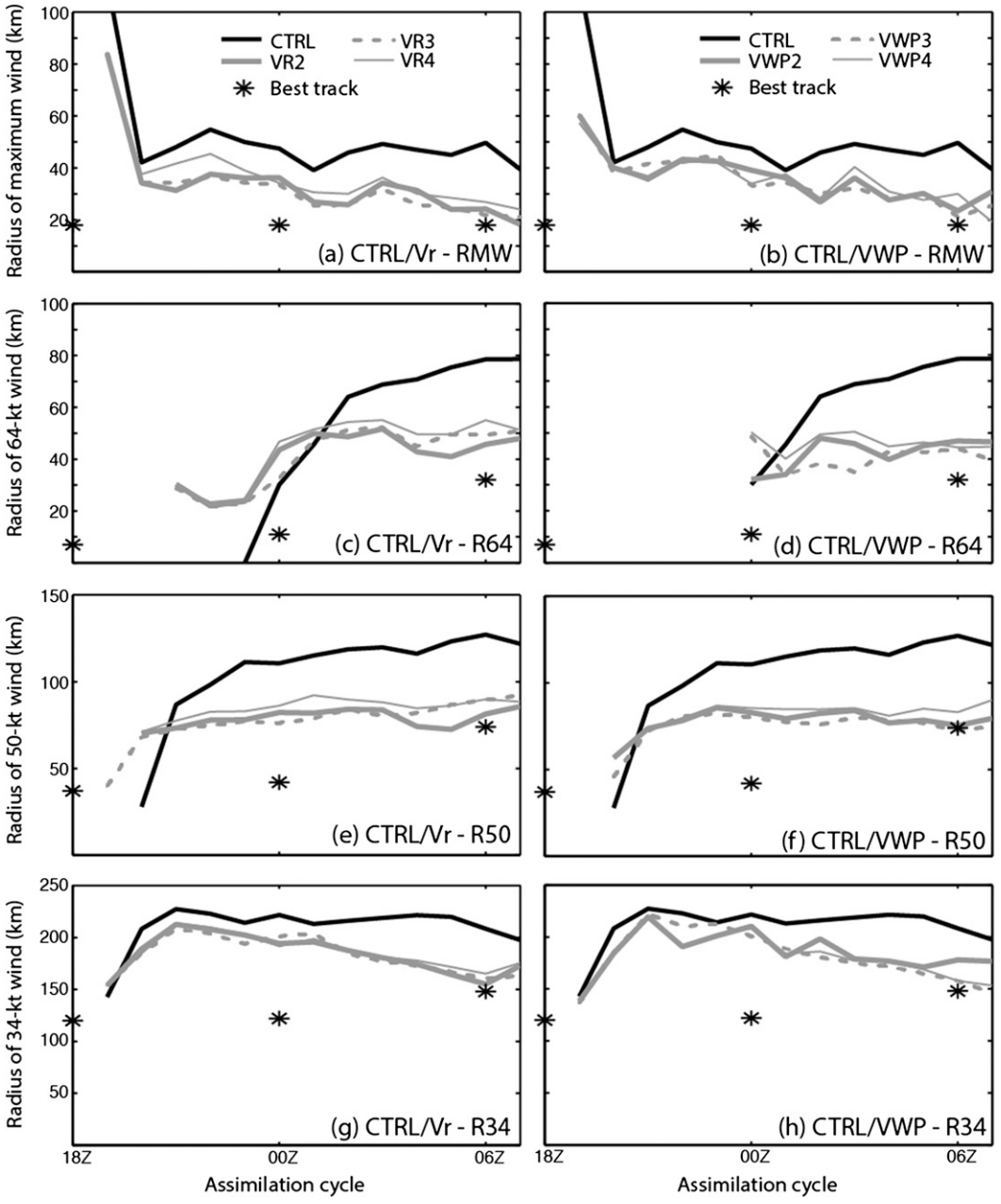

FIG. 6. The evolution of wind radii in the best track data compared to the various EnKF analyses. With the exception of the RMW, radii are computed as the maximum extent of winds of the given threshold (up to 300 km) in each quadrant, and the average value from the four quadrants is plotted. No data were plotted when analysis winds do not exceed the given threshold in any quadrant. The RMW is the distance from the storm center to the location of local maximum winds.

than in Fig. 7). Finally, Fig. 13 shows 3-km reflectivity at the final analysis cycle for comparison with Fig. 8. In general, the distribution of precipitation in the Vr experiments (left-hand column) is somewhat more like the Alvarado radar image than is CTRL. All three Vr-assimilating analyses have more compact inner-core precipitation structures than does CTRL. In addition, these analyses are generally more accurate in depicting Karl's asymmetric precipitation structure at the time.

A notable aspect of the Vr analyses is that they are all quite similar in terms of intensity and mean properties, and the same is true of the spread and error of the prior perturbations in these experiments. To demonstrate this, Fig. 14a shows the spread of the prior as

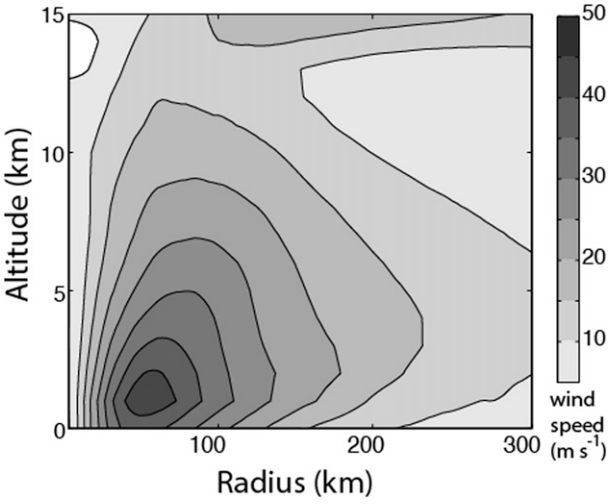

FIG. 7. Azimuthal mean wind speeds as a function of radius and altitude from CTRL at the final cycle time, 0700 UTC 17 Sep.

well root-mean-square error between the prior and independent Vr observations for all analysis cycles on 17 September (no Vr observations are available at 0300 UTC). During most cycles, all three Vr experiments are within about 1.0 m s^{-1} of each other in terms of root-mean-square error (RMSE), and they are even closer in terms of spread. This result is consistent with the findings of Weng and Zhang (2012), who found that Vr-assimilating analyses in Hurricane Katrina were generally insensitive to the assumed observation error.

The one metric by which the experiments are not congruent with one another is in the consistency between RMSE, ensemble spread, and assumed observation error, as evaluated by Eq. (9) from Aksoy et al. (2009):

$$R = \frac{\text{spread}}{\sqrt{\text{RMSE}^2 - \sigma^2}},$$

where σ is the specified observation error. As noted in Aksoy et al. (2009), the proper specification of observation error is crucial for interpretation of this ratio, and this appears to become an issue for experiment VR4. The ratio is optimally 1.0; when it is less than 1.0 the ensemble is underdispersive, and when it is greater than 1.0 the ensemble is overdispersive. Figure 14b, which shows R for the 17 September priors, indicates that VR2 comes closest to being optimal among the Vr-assimilating experiments. In VR3 R is slightly larger, but in VR4 it is very large. In fact, at the 0200 UTC cycle, the RMSE is less than the observation error so that R is not a real number. These results suggest that the specified error in VR4 is too large and that the most appropriate value is 2–3 m s^{-1}.

c. *VWP assimilation*

The analyses in the three VWP-assimilating experiments are also superior to CTRL, though they do not match some of the best track metrics quite as well as do the Vr experiments. In terms of maximum intensity, Figs. 9–10 show that the cyclones in the VWP experiments are slightly more intense than that in CTRL and slightly weaker than those in the Vr experiments. Though the cyclone tracks in the VWP experiments are very similar to those in the Vr experiments (Fig. 11), Fig. 5 reveals that they do have somewhat larger location error. Nevertheless, by the end of the assimilation period the location error is still much less than the specified observation error for storm position. Meanwhile, in terms of storm size, there is very little difference between the analyses assimilating VWP data and those assimilating Vr data. The largest discrepancy is during the first 6 hours, when the VWP analyses are slower to spin up the strongest winds, but the analyses are all very

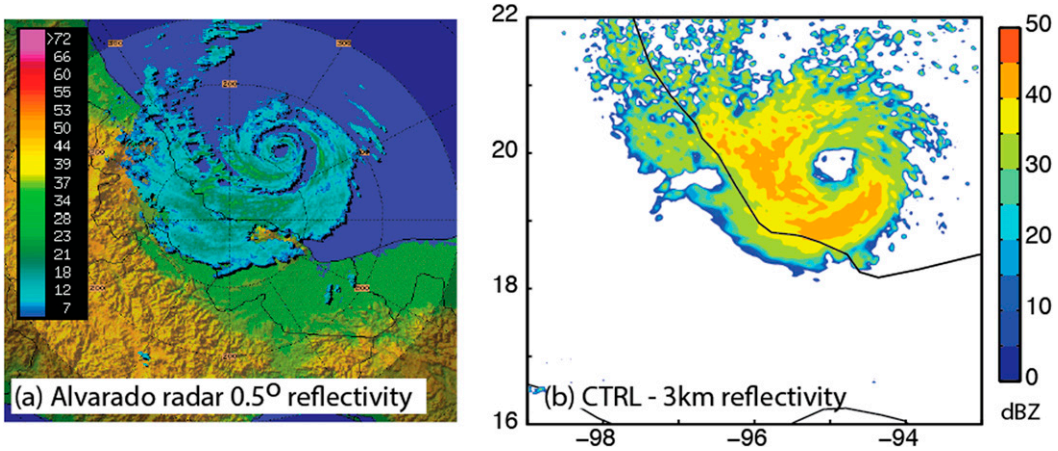

FIG. 8. A comparison of radar reflectivity from (a) the Alvarado radar 0.5° elevation angle and (b) the 3-km altitude in CTRL. Distance scales in both images are approximately the same to facilitate comparison.

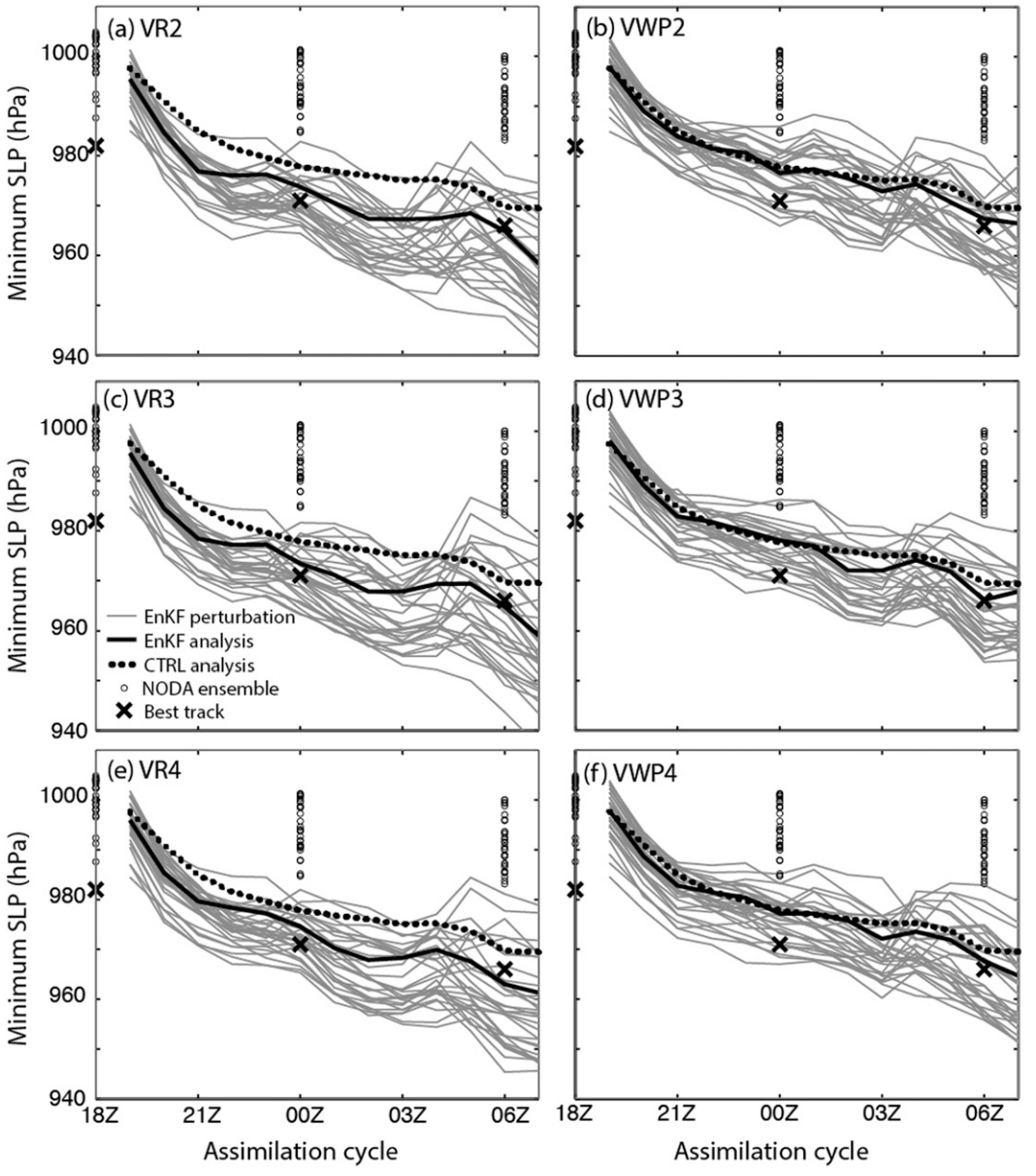

FIG. 9. As in Fig. 4a, but for the Vr- and VWP-assimilating experiments. The CTRL analysis mean is also shown for reference.

similar by 0000 UTC 17 September. Likewise, Fig. 12 reveals that the VWP experiments are also able to strengthen the cyclone circulation through the upper troposphere. The main difference between the Vr-assimilating experiments and the VWP-assimilating experiments is that the azimuthally averaged winds in VWP3 and VWP4 are about 5 m s^{-1} weaker (Figs. 12d,f). Finally, Fig. 13 shows that the precipitation distribution in the VWP experiments is somewhat different than in the Vr experiments. The storms in VWP3 and VWP4 are more symmetric (Figs. 13d,f) and thus somewhat less accurate on the system scale. However, all three VWP experiments have more complete eyewalls and generally better depictions of the inner core when compared with Fig. 8a.

One interesting difference between the VWP and Vr experiments is in the ensemble distribution for the maximum intensity metrics. For example, Fig. 9 shows that the VWP-assimilating analyses have considerably lower spread in minimum SLP by the final few assimilation cycles. In addition, Fig. 10 shows that the maximum winds in the ensemble members of the VWP

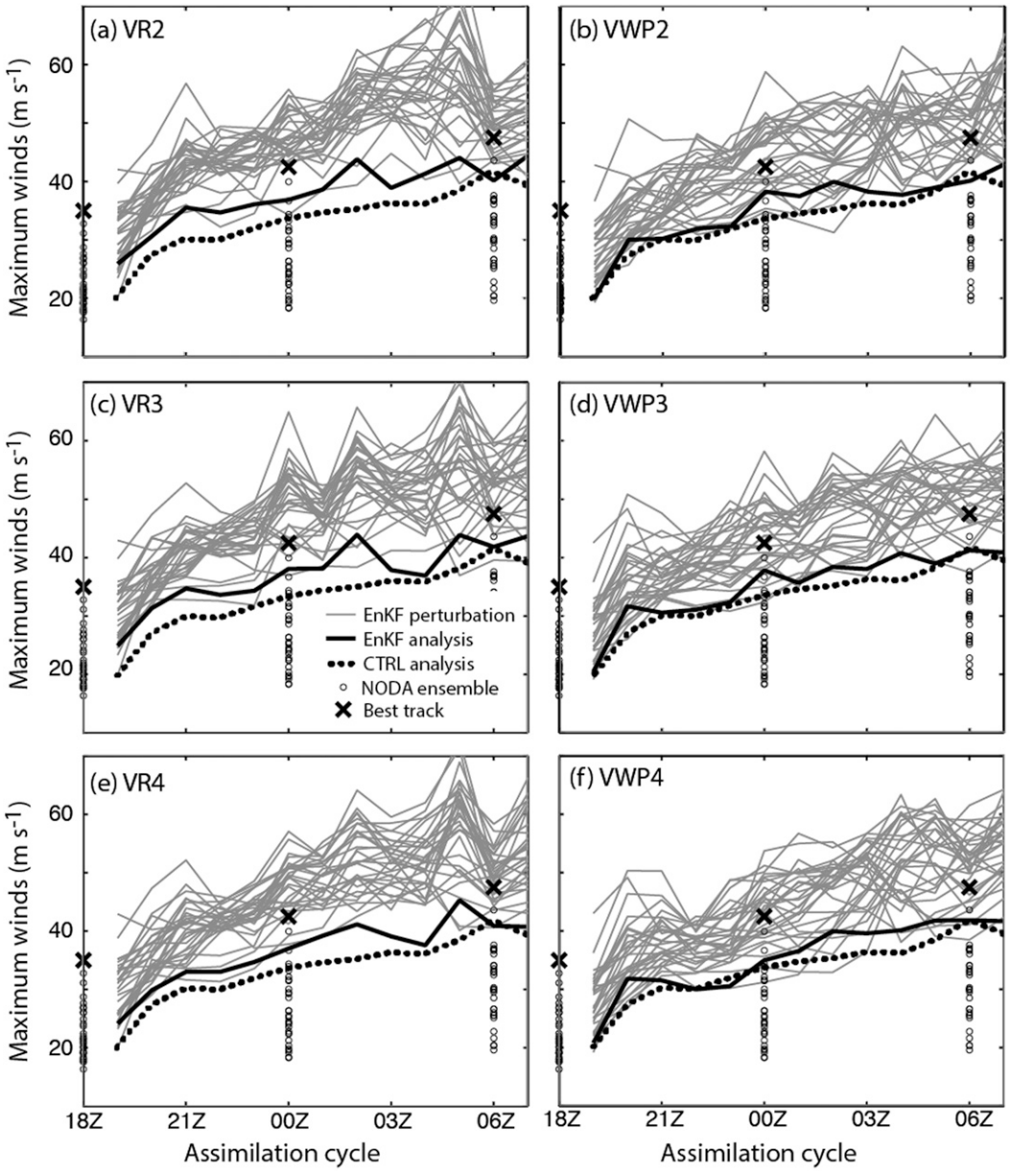

FIG. 10. As in Fig. 4b, but for the Vr- and VWP-assimilating experiments. The CTRL analysis mean is also shown for reference.

experiments tend to be closer to analysis mean itself. These differences are reflective of the fact that there is considerably more variation in cyclone structure in the Vr experiments (not shown), which might be a result of noisier error covariance in those analyses.

The VWP-assimilating experiments also behave somewhat differently than the Vr experiments in terms of prior spread and error. Figure 15a shows the spread and error in the VWP experiments evaluated against the same set of independent Vr data that were used in Fig. 14a (Vr data were chosen instead of VWP data so that the results would be directly comparable). Whereas there is fairly strong nonmonotonic variation in RMSE in the Vr experiments, in the VWP experiments the error tends to decrease with time. In terms of spread consistency, the VWP-assimilating experiments are somewhat better behaved than the Vr experiments. The consistency ratio R (evaluated assuming σ for Vr is $2\,\mathrm{m\,s^{-1}}$, though results are similar for $\sigma = 3\,\mathrm{m\,s^{-1}}$) in all three VWP experiments is around 0.75 at 0000 UTC 17 September, and it gradually increases to about 1.2 by the final cycle (Fig. 15b).

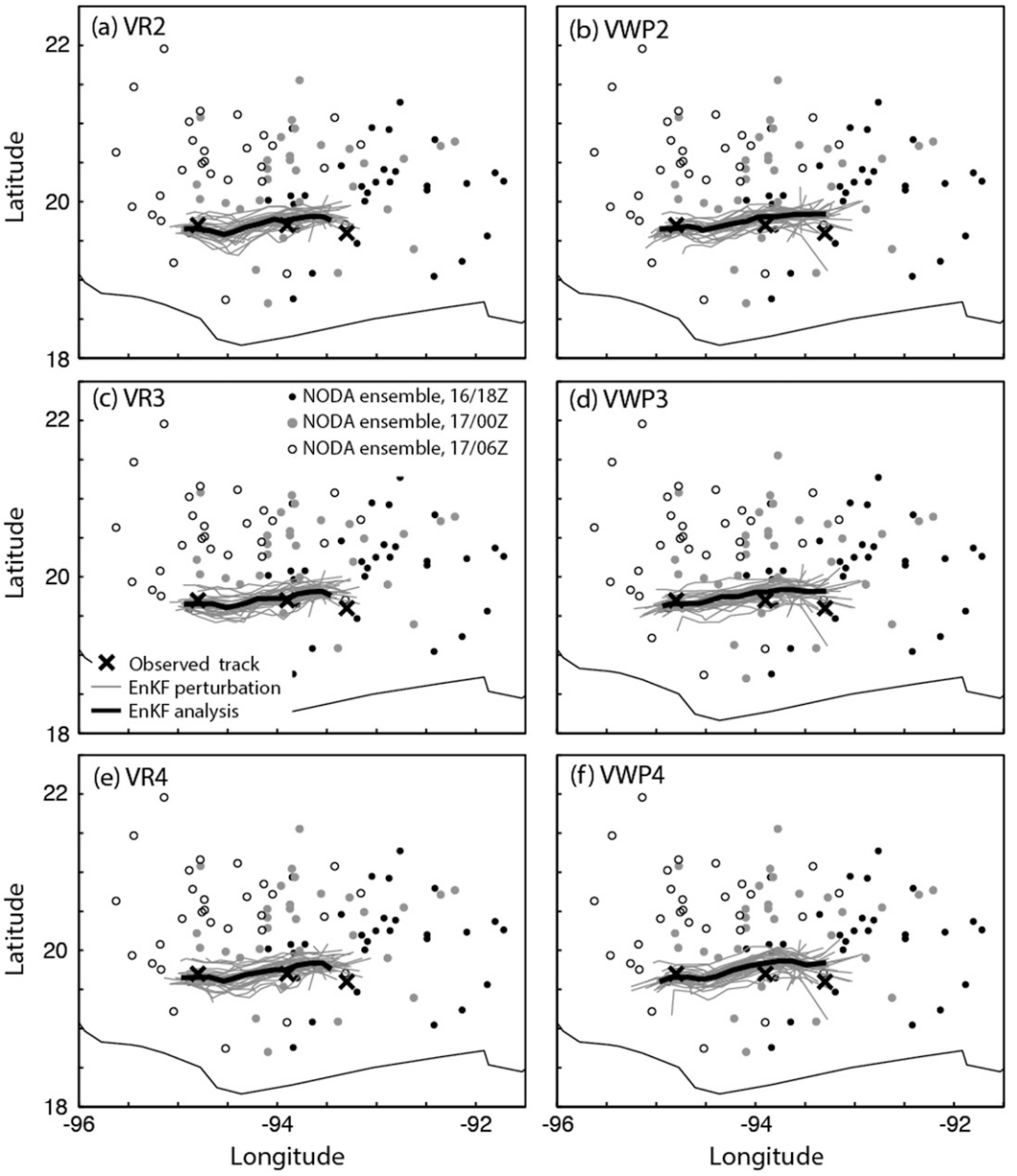

FIG. 11. As in Fig. 4c, but for the Vr- and VWP-assimilating experiments.

d. EnKF-initialized deterministic forecasts

When evaluating a data assimilation system, it is important to examine both the improvement in the analysis and the ultimate forecast improvement. As such, this section compares short-term deterministic forecasts initialized from the EnKF analyses with the best track data and the NODA deterministic forecast. Forecasts are initialized at 0000, 0200, 0400, and 0600 UTC 17 September to give a sense of how forecasts evolve as assimilation continues. Results are shown in Figs. 16–18 for intensity and track. In addition, for each Vr and VWP experiment the four above forecasts are used to calculate a mean forecast track and intensity at 1200 and 1800 UTC 17 September, and the error of the calculated mean is shown in Table 2.

The most important result is that the EnKF-initialized forecasts are vast improvements upon NODA. Without assimilation, the forecast produces a storm that is much weaker than the observed cyclone (Figs. 16 and 17). In addition, Fig. 18 shows that the storm in NODA moves too slowly and too far north, never making the southwest turn before landfall. However, all EnKF-initialized forecasts have an intensity evolution that looks much

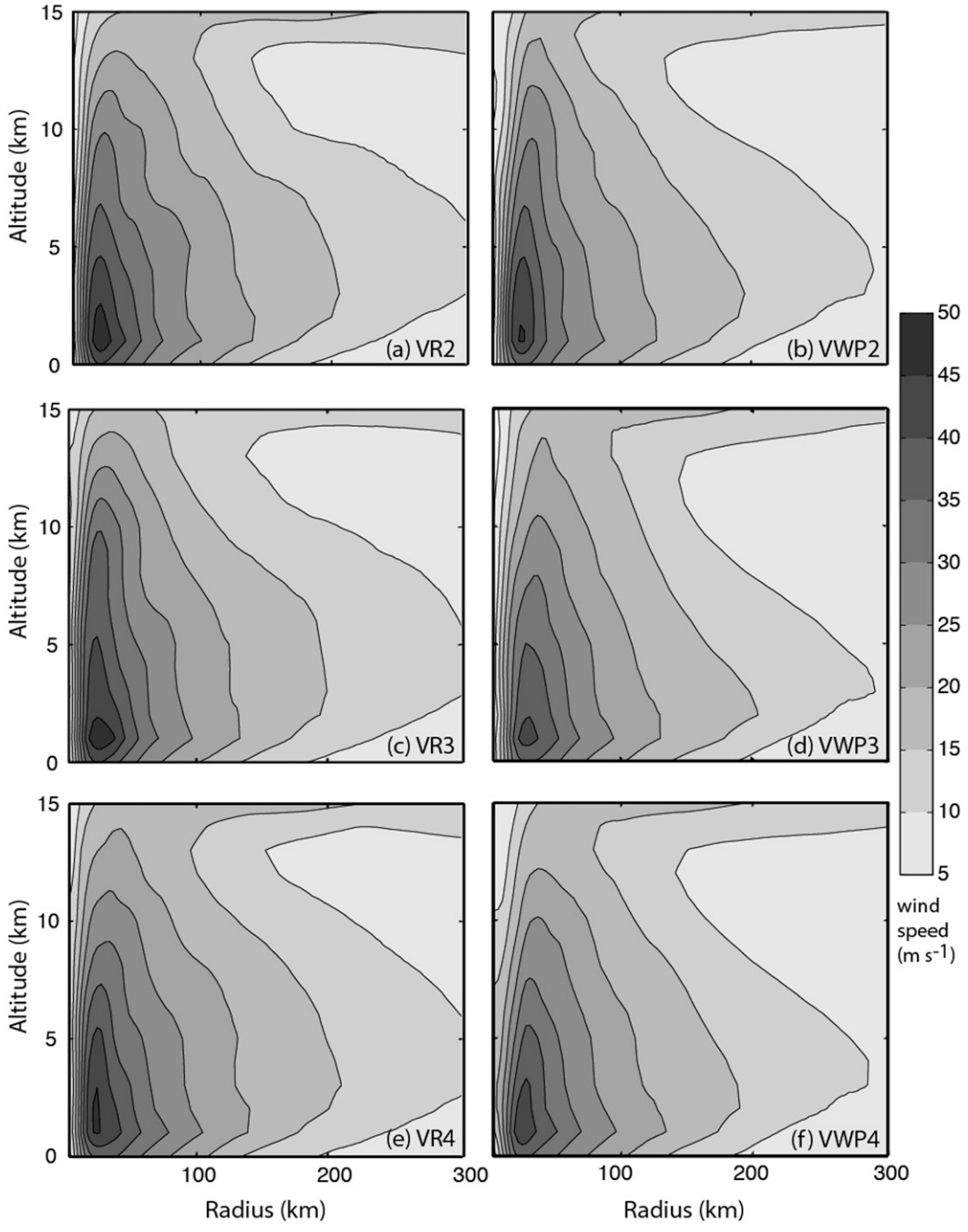

FIG. 12. As in Fig. 7, but for the Vr- and VWP-assimilating experiments.

more like the best track data, and they all take the correct turn before landfall.

Among the EnKF-initialized forecasts, those initialized from CTRL generally perform the worst. The major problem with forecasts initialized from CTRL is a dramatic adjustment that ensues from the broad, shallow circulation. Though maximum winds from CTRL-initialized forecasts generally come within about 5 m s^{-1} of the best track wind data (Fig. 17), the evolution of surface pressure in Fig. 16 is wrong. Instead of continuing to decrease, the pressure in these forecasts stays steady or increases, which is symptomatic of the aforementioned adjustment. This is in contrast to almost all of the forecasts initialized from analyses that assimilate HIWRAP data, where minimum SLP decreases as the maximum winds increase.

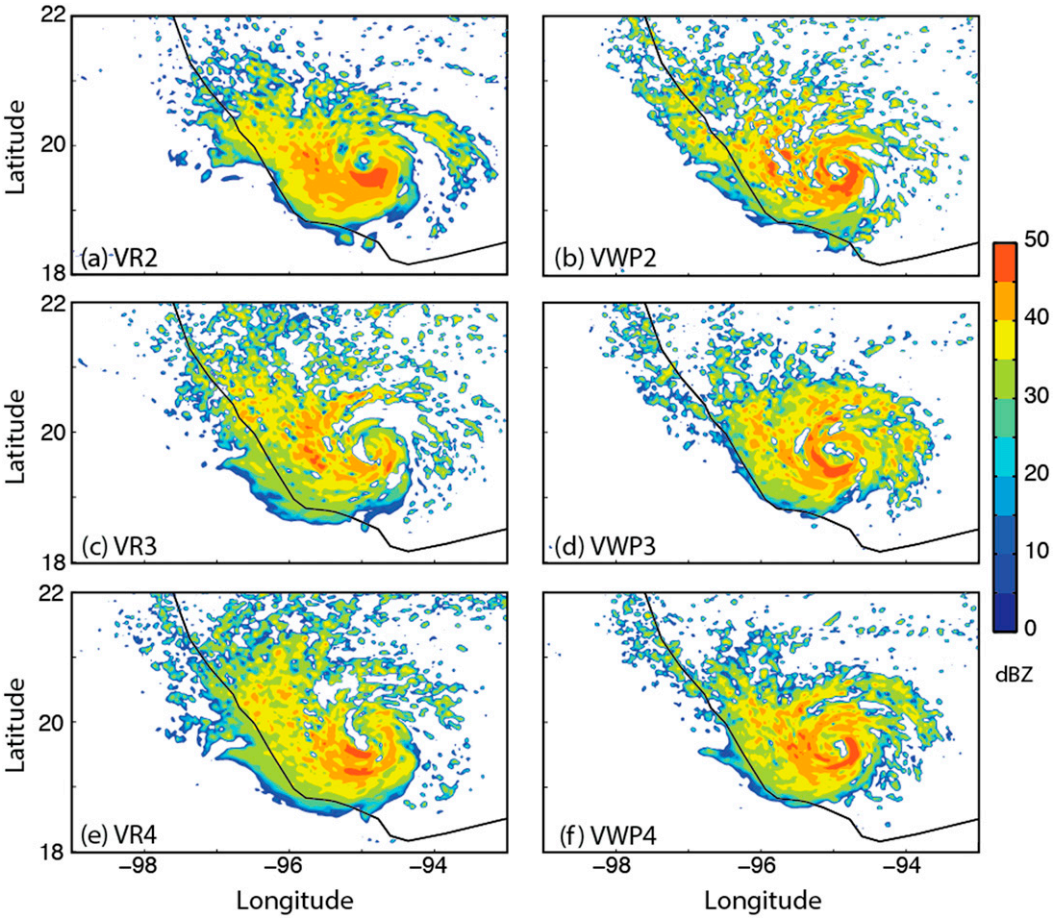

FIG. 13. As in Fig. 8b, but for the Vr- and VWP-assimilating experiments. Length scales are the same as in Fig. 8, but domains have been trimmed.

Forecasts initialized from the VWP experiments perform slightly better than do those initialized from the Vr experiments. One problem with forecasts from the Vr-assimilating analyses is that they generally intensify the maximum winds to be about 5–10 m s^{-1} stronger than what was observed. This is particularly evident in forecasts initialized from VR2, which generally contain the strongest hurricane among all the experiments (Figs. 16–17 and Table 2). Meanwhile, the VWP-initialized forecasts of maximum wind speed are almost always within about 5 m s^{-1} of the best track estimate. Though Table 2 shows that the minimum SLP predicted from the Vr-initialized forecasts is more accurate near the time of maximum intensity at 1200 UTC, by 1800 UTC the minimum SLP error in these forecasts is much larger. Forecasts from the VWP experiments are also superior to those from Vr experiments in terms of track, which is most evident in Table 2. Track error is about 20% lower in the VWP-initialized forecasts, which could suggest that the horizontal VWP wind estimates are more able to correct the larger-scale wind fields.

Curiously, the most inaccurate forecasts of maximum wind speed from both the Vr and VWP experiments are those initialized near the end of the analysis period. The deterministic forecasts from all six experiments that assimilate HIWRAP data produce a storm more than 5 m s^{-1} stronger than the maximum intensity observed from Karl. This is a time when the flight strategy of the Global Hawk changed from surveillance of the entire storm to a focus on the inner core. It is possible that this shift in strategy impacts both the analyses and the subsequent forecasts, though an investigation of this is beyond the scope of this study.

It is also interesting that the differences between the forecasts from the Vr experiments are somewhat larger than the differences from the VWP experiments. The differences are most pronounced in the forecasts initialized at 0000 and 0200 UTC, where there is substantial variability in the Vr-initialized forecast intensity and track metrics in Figs. 16–18. This could be another result of noisier error covariance during the assimilation of Vr.

While the forecasts from the Vr-assimilating analyses are not as good as those in the simulated-data study of S13,

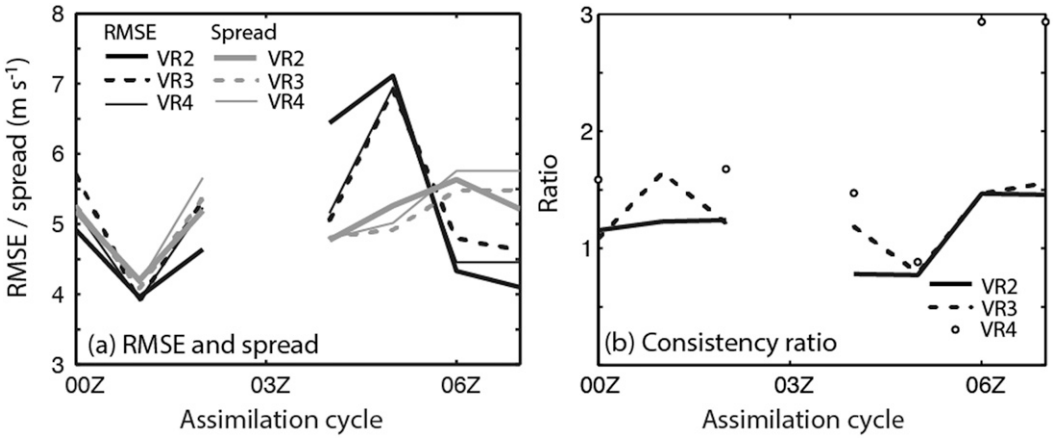

FIG. 14. The evolution of (a) RMSE and prior spread and (b) the consistency ratio *R* between spread, RMSE, and observation error for the three Vr-assimilating experiments. The metrics are calculated from the priors of the assimilation cycles from 0000 to 0700 UTC 17 Sep against a set of independent Vr observations. No Vr data were available from the 0300 UTC cycle.

this is expected given the differences between the studies. Likely causes for the discrepancy between these results and those of S13 include the larger elevation angle used here and the presence of larger model error in this real-data situation. Given the lack of HIWRAP data from other hurricanes, it is currently impossible to ascertain whether or not assimilation will be more successful with outer-beam Vr assimilation. Nevertheless, the forecasts initialized from the VWP experiments are encouraging. The slight improvement upon the Vr experiments is likely a result of assimilating two horizontal components of the wind and circumventing the need to rely strongly on error covariance that is impacted by vertical velocity.

4. Conclusions

This study examines the potential usefulness of assimilating Doppler velocity (Vr) and Doppler-derived VAD wind profile (VWP) data gathered from an unmanned aircraft for hurricane analysis. Thinned and quality-controlled HIWRAP radar observations of Hurricane Karl (2010) were assimilated with a WRF-EnKF system that has successfully been used in the past for hurricane analysis and forecasting. HIWRAP flew on the Global Hawk during the GRIP experiment, and this is the first study to use this data in assimilation experiments. Currently, Karl is the only hurricane for which HIWRAP are available, though the radar is being used in the ongoing HS3 experiment. This study is intended as a follow-up to S13, which extensively examined this topic with simulated-data experiments. Previous studies have shown that airborne radar data can be useful for hurricane initialization, but it has never before been attempted with data obtained from a high-altitude radar.

Karl was the first hurricane from which HIWRAP data were gathered, and as in many first-time operations,

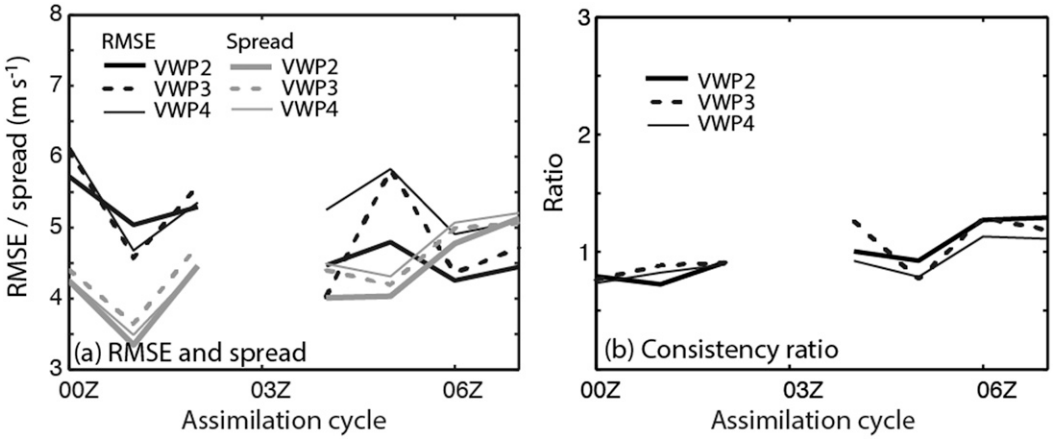

FIG. 15. As in Fig. 14, but for the three VWP-assimilating experiments.

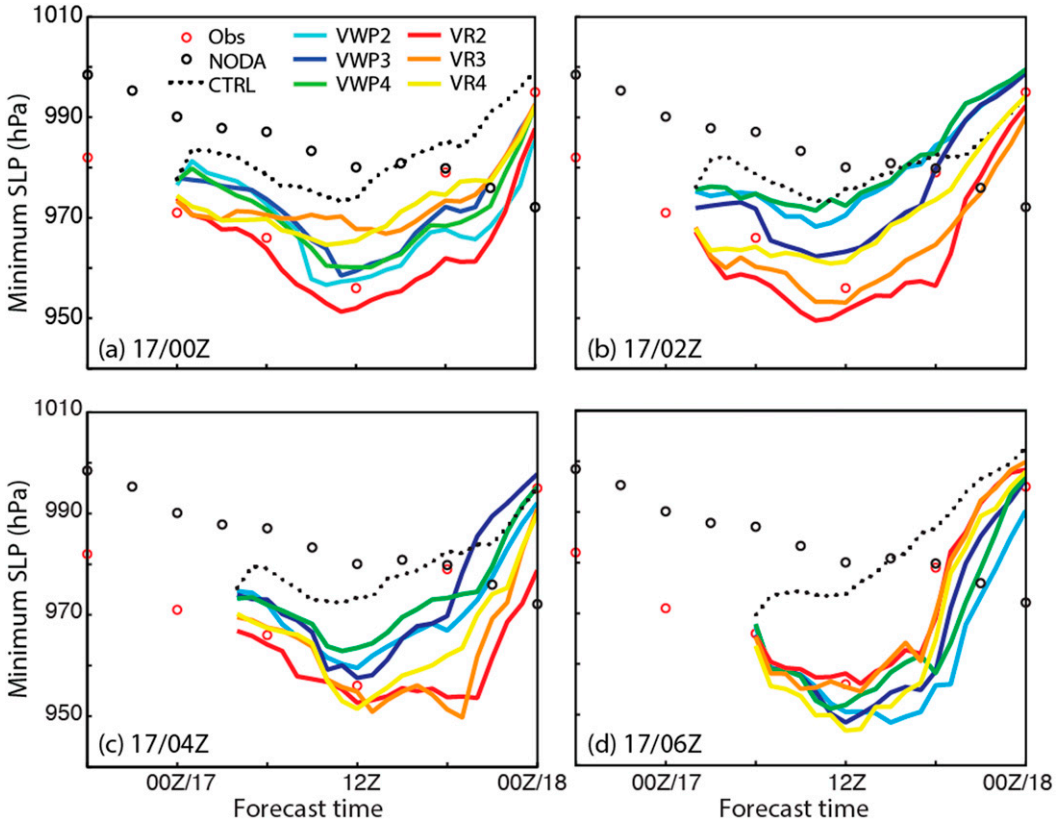

FIG. 16. The evolution of best track minimum SLP compared to that from NODA and deterministic forecasts initialized from the EnKF analyses at (a) 0000, (b) 0200, (c) 0400, and (d) 0600 UTC 17 Sep.

a number of problems arose that negatively impacted data quality. Foremost, only inner-beam (30° incidence) HIWRAP data were available from the flight, which is a major disadvantage compared to the S13 simulated-data experiments. That study assumed use of the outer beam (40° incidence), which measures less of the vertical component of the wind and is more desirable for data assimilation because of the diminished potential for noisy or erroneous sample covariance. The Doppler data from Karl were also contaminated with noise that required strict quality control to correct, and accurate velocity unfolding was not possible for several legs. These problems have since been addressed, and we anticipate less stringent quality-control requirements for future HIWRAP missions.

An alternative to directly assimilating Vr is to assimilate the estimated horizontal wind components from a VWP analysis. In this case, the HIWRAP VWP data were produced from the methods outlined in T14. Potential benefits of this approach include circumventing fall speed correction in addition to avoiding noisy or inaccurate error covariance associated with vertical velocity. In addition, the VWP method provides two horizontal components of the wind, which might more easily constrain the horizontal wind field. A potential pitfall comes in the assumptions used in calculating the VWP components. To the best of our knowledge, this method has not previously been attempted for hurricane assimilation.

The data problems with the flight into Karl encouraged the assimilation of position and intensity every hour in addition to the HIWRAP data, which was not required with S13. This step helps constrain the analysis during cycles when little or no data are available. Though this step is not strictly necessary, it does help spin up the vortex faster.

An experiment assimilating only position and intensity was performed in order to establish a baseline upon which assimilating HIWRAP data can improve the analyses and subsequent forecasts. This experiment, CTRL, does a good job at constraining the vortex location and maximum intensity, but it is not able to correctly analyze the vortex size or depth. Thus, cyclones in deterministic forecasts initialized from CTRL undergo large adjustments so that their subsequent structural evolution is incorrect. Despite this problem, these

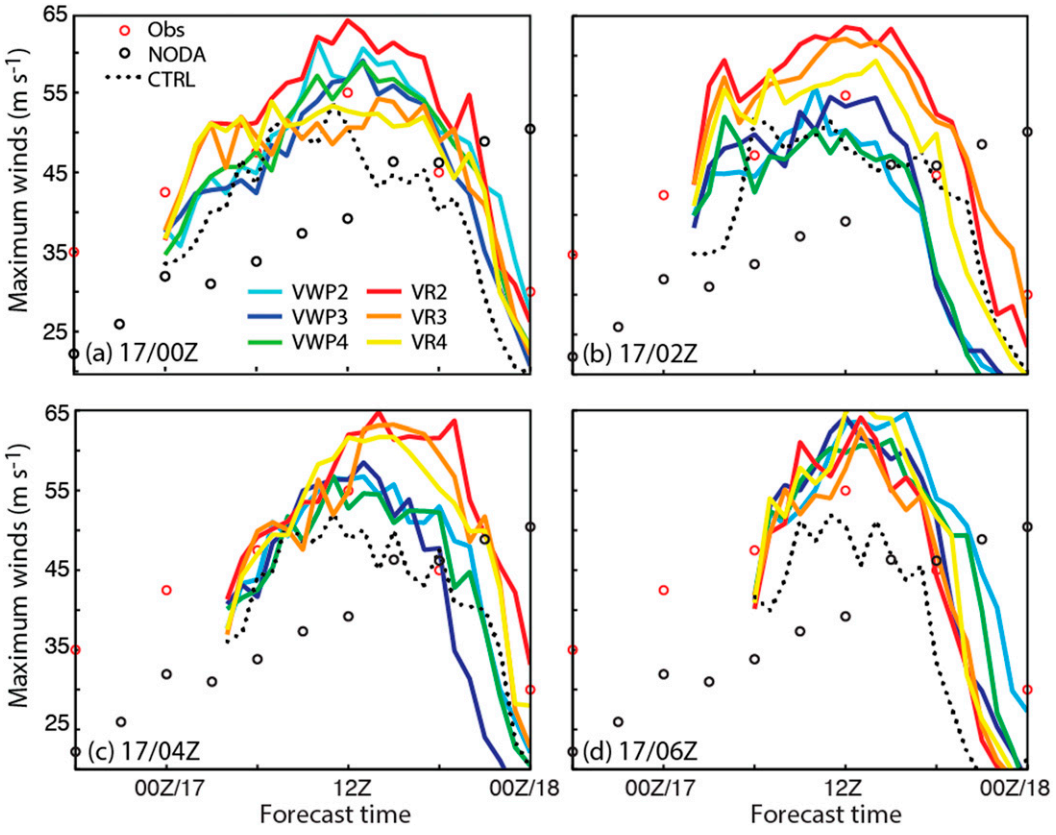

FIG. 17. As in Fig. 16, but for maximum wind speed.

forecasts are significantly better than a forecast without any assimilation in terms of both cyclone intensity and track. In particular, the CTRL-initialized forecasts correctly capture Karl's west and southwest turn before landfall, which is completely missed when no data are assimilated.

The experiments that assimilate HIWRAP data significantly improve upon CTRL, particularly where CTRL performs poorly. Maximum intensity is more accurate in these experiments, but the most significant improvement is in the size and depth of the analyzed storm. By the end of the assimilation period, the storms in the Vr and VWP experiments are all more compact than that in CTRL, which is in much better agreement with best track data. They also all have a vertical structure more consistent with available data and with the theoretical structure of a major hurricane, and their precipitation structure agrees better with available radar data.

Deterministic forecasts initialized from Vr and VWP-assimilating analyses improve upon those initialized from CTRL, and forecasts initialized from the VWP experiments are slightly more accurate than those initialized from the Vr experiments. The major adjustment that takes place in the CTRL-initialized forecasts is generally absent here, and the evolution of maximum winds and minimum SLP in these forecasts is more consistent with the best track data. In addition, the forecast track in these experiments accurately turns to the southwest, which is consistent with the CTRL forecasts. One problem with forecasts from the Vr experiments is that they generally intensify the maximum winds to about 5–10 $m\,s^{-1}$ stronger than what was observed. However, the VWP-initialized forecasts of maximum wind speed are generally within about 5 $m\,s^{-1}$ of the best track estimate. The VWP experiments also produce more accurate forecasts of cyclone track.

It is interesting that the VWP-initialized forecasts are more accurate than the Vr-initialized forecasts despite the fact that the Vr-assimilating analyses better match the best track data. The most plausible explanation for this is that storm environment is more accurate in the VWP analyses, which is suggested by the larger track error from the Vr-initialized forecasts. This may be a result of poorer forecast error covariance for Vr than for VWP. It is also possible that the analyses that assimilate Vr are more inaccurate in ways that are not captured here.

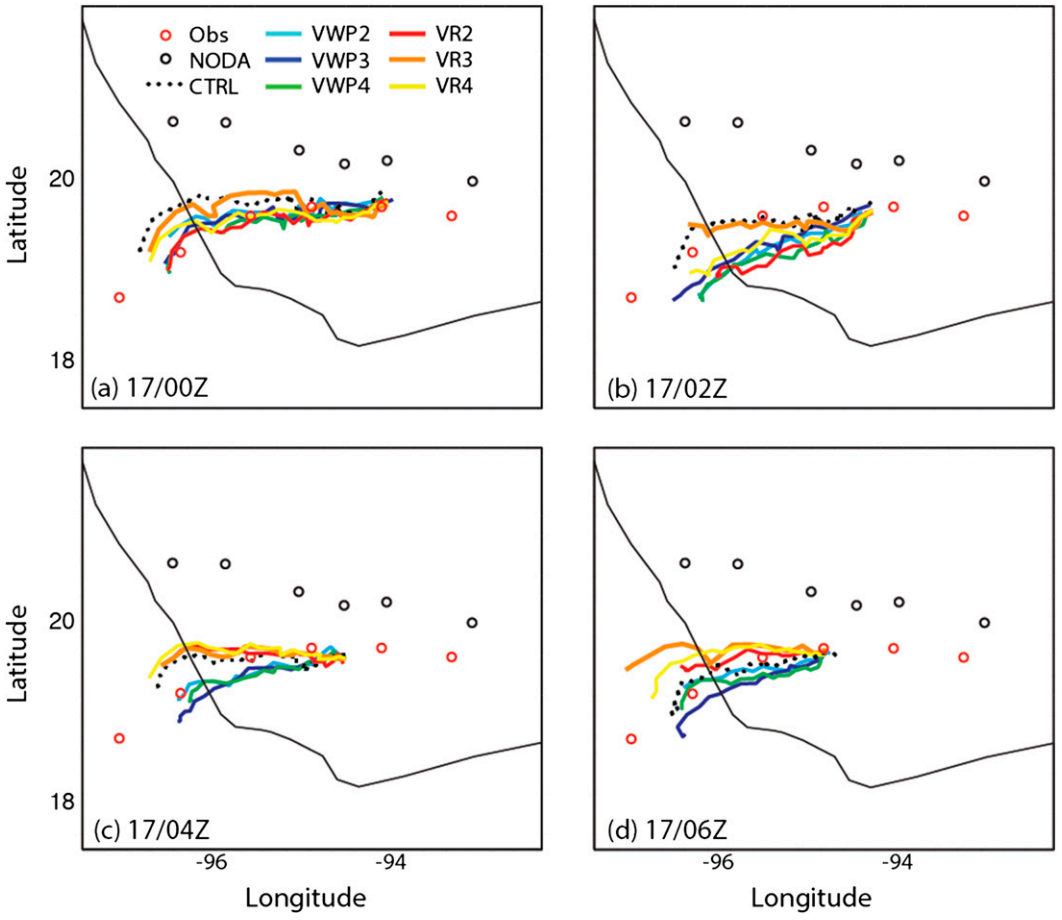

FIG. 18. As in Fig. 16, but for cyclone track. The best track and NODA locations are plotted every 6 h.

While the forecasts initialized from the Vr experiments are not as good as those in S13, this is expected given the differences between the studies. Likely causes for the discrepancy between these results and those of S13 include the larger elevation angle used here and the presence of larger model error in this real-data situation. Given the lack of HIWRAP data from other hurricanes, it is currently impossible to ascertain whether or not assimilation will be more successful with outer-beam Vr data. Also, though the VWP-initialized forecasts are slightly better in this situation, it is not clear that this will always be the case. It is possible when outer-beam HIWRAP data are available that Vr assimilation will outperform that of VWP estimates.

The appropriate number of observations here is rather low compared to other recently published Vr-assimilating studies (e.g., Zhang et al. 2009; Aksoy et al. 2013), perhaps due to differences in radar geometry. The HIWRAP observations are constrained to a generally small area following the aircraft track, whereas Vr observations from ground-based radars or the NOAA P3 can potentially cover the entire volume occupied by a storm. Ultimately the appropriate number of observations here *should be* substantially fewer than that from previously published studies where the data occupy a much larger volume. Yet, the number of Vr observations assimilated here is a small fraction of that even in S13, which assumed the HIWRAP geometry. The use of such a low number of Vr observations here was motivated by the consistency between ensemble spread and error; if more observations were assimilated, the analyses tended to have error lower than the spread. It is possible that the number of observations assimilated in S13 was too large, as that study never examined the spread–error consistency.

In summary, although the data quality from the GRIP HIWRAP flights presented a number of obstacles, the results from this study show that a relatively small amount of HIWRAP data can be useful for hurricane analysis and forecasting. Future work needs to examine if these results are applicable to other storms as more HIWRAP data become available. The radar is currently

TABLE 2. Mean intensity and track errors from the EnKF-initialized forecasts valid at 1200 and 1800 UTC 17 Sep. The means are computed across the four forecasts from each experiment (i.e., initialized at 0000, 0200, 0400, and 0600 UTC) shown in Figs. 16–18. The mean of the absolute error (MAE) at the two verification times in each experiment is shown below the 1800 UTC rows. Also, the MAE at each verification time for the VR and VWP experiment sets appears to the right of each set of experiments. Errors have been rounded to the nearest significant digit.

	VR2	VR3	VR4	MAE	VWP2	VWP3	VWP4	MAE
Wind speed ($m\,s^{-1}$)								
1200 UTC	8	2	4	4	2	3	0	2
1800 UTC	8	7	6	7	2	0	2	2
MAE	8	5	5		2	2	1	
Min SLP (hPa)								
1200 UTC	−3	2	0	2	4	1	6	4
1800 UTC	−18	−14	−10	14	−10	−9	−8	9
MAE	12	8	5		7	5	7	
Track (km)								
1200 UTC	44	46	46	45	35	35	43	38
1800 UTC	58	61	55	58	47	32	50	43
MAE	51	54	51		41	34	47	

being used for the HS3 field campaign, which should allow for further tests in the near future. Since many of the problems associated with the early HIWRAP datasets have now been resolved, the stringent quality-control procedures required here should be alleviated to allow for even greater usefulness of this data.

Acknowledgments. The authors are thankful for discussions with Frank Marks, Stephen Guimond, and Altug Aksoy. This manuscript also benefited from comments from three anonymous reviewers and the editor, Dr. Jeffrey Anderson. Funding for this work came from the NASA Hurricane Sciences Research Program under Dr. Ramesh Kakar, the Hurricane and Severe Storm Sentinel Investigation under NASA's Earth Venture Program, and the NASA New Investigator Program. The simulations were conducted on NASA Center for Climate Simulation facilities.

REFERENCES

Aksoy, A., D. C. Dowell, and C. Snyder, 2009: A multicase comparative assessment of the ensemble Kalman filter for assimilation of radar observations. Part I: Storm-scale analyses. *Mon. Wea. Rev.,* **137,** 1805–1824, doi:10.1175/2008MWR2691.1.

——, S. Lorsolo, T. Vukicevic, K. J. Sellwood, S. D. Aberson, and F. Zhang, 2012: The HWRF Hurricane Ensemble Data Assimilation System (HEDAS) for high-resolution data: The impact of airborne Doppler radar observations in an OSSE. *Mon. Wea. Rev.,* **140,** 1843–1862, doi:10.1175/MWR-D-11-00212.1.

——, S. D. Aberson, T. Vukicevic, K. J. Sellwood, S. Lorsolo, and X. Zhang, 2013: Assimilation of high-resolution tropical cyclone observations with an ensemble Kalman filter using NOAA/AOML/HRD's HEDAS: Evaluation of the 2008–11 vortex-scale analyses. *Mon. Wea. Rev.,* **141,** 1842–1865, doi:10.1175/MWR-D-12-00194.1.

Barker, D. M., W. Huang, Y.-R. Guo, A. J. Bourgeois, and Q. N. Xiao, 2004: A three-dimensional variational data assimilation system for MM5: Implementation and initial results. *Mon. Wea. Rev.,* **132,** 897–914, doi:10.1175/1520-0493(2004)132<0897:ATVDAS>2.0.CO;2.

Benjamin, S. G., and Coauthors, 2004: An hourly assimilation–forecast cycle: The RUC. *Mon. Wea. Rev.,* **132,** 495–518, doi:10.1175/1520-0493(2004)132<0495:AHACTR>2.0.CO;2.

——, B. D. Jamison, W. R. Moninger, S. R. Sahm, B. E. Schwartz, and T. W. Schlatter, 2010: Relative short-range forecast impact from aircraft, profiler, radiosonde, VAD, GPS-PW, METAR, and mesonet observations via the RUC hourly assimilation cycle. *Mon. Wea. Rev.,* **138,** 1319–1343, doi:10.1175/2009MWR3097.1.

Braun, S. A., and Coauthors, 2013: NASA's Genesis and Rapid Intensification Processes (GRIP) Field Experiment. *Bull. Amer. Meteor. Soc.,* **94,** 345–363, doi:10.1175/BAMS-D-11-00232.1.

Browning, K. A., and R. Wexler, 1968: The determination of kinematic properties of a wind field using Doppler radar. *J. Appl. Meteor.,* **7,** 105–113, doi:10.1175/1520-0450(1968)007<0105:TDOKPO>2.0.CO;2.

Dong, J., and M. Xue, 2013: Assimilation of radial velocity and reflectivity data from coastal WSR-88D radars using an ensemble Kalman filter for the analysis and forecast of landfalling Hurricane Ike (2008). *Quart. J. Roy. Meteor. Soc.,* **139,** 467–487, doi:10.1002/qj.1970.

Dudhia, J., 1989: Numerical study of convection observed during the winter monsoon experiment using a mesoscale two-dimensional model. *J. Atmos. Sci.,* **46,** 3077–3107, doi:10.1175/1520-0469(1989)046<3077:NSOCOD>2.0.CO;2.

Gaspari, G., and S. E. Cohn, 1999: Construction of correlation functions in two and three dimensions. *Quart. J. Roy. Meteor. Soc.,* **125,** 723–757, doi:10.1002/qj.49712555417.

Hawkins, H. F., and S. M. Imbembo, 1976: The structure of a small, intense hurricane—Inez 1966. *Mon. Wea. Rev.,* **104,** 418–442, doi:10.1175/1520-0493(1976)104<0418:TSOASI>2.0.CO;2.

Heymsfield, G., L. Tian, A. J. Heymsfield, L. Li, and S. Guimond, 2010: Characteristics of deep tropical and subtropical convection from nadir-viewing high-altitude airborne Doppler radar. *J. Atmos. Sci.,* **67,** 285–308, doi:10.1175/2009JAS3132.1.

Hong, S.-Y., J. Dudhia, and S.-H. Chen, 2004: A revised approach to ice-microphysical processes for the bulk parameterization

of cloud and precipitation. *Mon. Wea. Rev.,* **132,** 103–120, doi:10.1175/1520-0493(2004)132<0103:ARATIM>2.0.CO;2.

Kain, J. S., and J. M. Fritsch, 1990: A one-dimensional entraining/detraining plume model and its application in convective parameterization. *J. Atmos. Sci.,* **47,** 2784–2802, doi:10.1175/1520-0469(1990)047<2784:AODEPM>2.0.CO;2.

——, and ——, 1993: Convective parameterization for mesoscale models: The Kain-Fritsch scheme. *The Representation of Cumulus Convection in Numerical Models, Meteor. Monogr.,* No. 24, Amer. Meteor. Soc., 165–170.

Landsea, C. W., and J. L. Franklin, 2013: Atlantic hurricane database uncertainty and presentation of a new database format. *Mon. Wea. Rev.,* **141,** 3576–3592, doi:10.1175/MWR-D-12-00254.1.

Lhermitte, R. M., and D. Atlas, 1961: Precipitation motion by pulse Doppler radar. *Proc. Ninth Weather Radar Conf.,* Kansas City, MO, Amer. Meteor. Soc., 218–223.

Li, L., G. Heymsfield, J. Carswell, D. Schaubert, M. Mclinden, M. Vega, and M. Perrine, 2011: Development of the NASA High-Altitude Imaging Wind and Rain Airborne Profiler (HIWRAP) for tropical storm research. Preprints, *IEEE Aerospace Conf.,* Big Sky, MT, IEEE, Paper 6.0202, 7 pp.

Marks, F. D., Jr., and R. A. Houze Jr., 1987: Inner core structure of Hurricane Alicia from airborne Doppler radar observations. *J. Atmos. Sci.,* **44,** 1296–1317, doi:10.1175/1520-0469(1987)044<1296:ICSOHA>2.0.CO;2.

Meng, Z., and F. Zhang, 2008a: Tests of an ensemble Kalman filter for mesoscale and regional-scale data assimilation. Part III: Comparison with 3DVAR in a real-data case study. *Mon. Wea. Rev.,* **136,** 522–539, doi:10.1175/2007MWR2106.1.

——, and ——, 2008b: Tests of an ensemble Kalman filter for mesoscale and regional-scale data assimilation. Part IV: Comparison with 3DVAR in a real-data case study. *Mon. Wea. Rev.,* **136,** 3671–3682, doi:10.1175/2008MWR2270.1.

Michelson, S. A., and N. L. Seaman, 2000: Assimilation of NEXRAD-VAD winds in summertime meteorological simulations over the northeastern United States. *J. Appl. Meteor.,* **39,** 367–383, doi:10.1175/1520-0450(2000)039<0367:AONVWI>2.0.CO;2.

Mlawer, E. J., S. J. Taubman, P. D. Brown, M. J. Iacono, and S. A. Clough, 1997: Radiative transfer for inhomogeneous atmosphere: RRTM, a validated correlated-k model for the longwave. *J. Geophys. Res.,* **102,** 16 663–16 682, doi:10.1029/97JD00237.

Noh, Y., W.-G. Cheon, and S.-Y. Hong, 2003: Improvement of the K-profile model for the planetary boundary layer based on large eddy simulation data. *Bound.-Layer Meteor.,* **107,** 401–427, doi:10.1023/A:1022146015946.

Poterjoy, J., and F. Zhang, 2011: Dynamics and structure of forecast error covariance in the core of a developing hurricane. *J. Atmos. Sci.,* **68,** 1586–1605, doi:10.1175/2011JAS3681.1.

——, ——, and Y. Weng, 2014: The effects of sampling errors on the EnKF assimilation of inner-core hurricane observations. *Mon. Wea. Rev.,* **142,** 1609–1630, doi:10.1175/MWR-D-13-00305.1.

Sippel, J. A., S. A. Braun, F. Zhang, and Y. Weng, 2013: Ensemble Kalman filter assimilation of simulated HIWRAP Doppler velocity data in a hurricane. *Mon. Wea. Rev.,* **141,** 2683–2704, doi:10.1175/MWR-D-12-00157.1.

Weng, Y., and F. Zhang, 2012: Assimilating airborne Doppler radar observations with an ensemble Kalman filter for convection-permitting hurricane initialization and prediction: Katrina (2005). *Mon. Wea. Rev.,* **140,** 841–859, doi:10.1175/2011MWR3602.1.

Zhang, F., C. Snyder, and J. Sun, 2004: Impacts of initial estimate and observation availability on convective-scale data assimilation with an ensemble Kalman filter. *Mon. Wea. Rev.,* **132,** 1238–1253, doi:10.1175/1520-0493(2004)132<1238:IOIEAO>2.0.CO;2.

——, Y. Weng, J. A. Sippel, Z. Meng, and C. H. Bishop, 2009: Convection-permitting hurricane initialization and prediction through assimilation of Doppler radar observations with an ensemble Kalman filter: Humberto (2007). *Mon. Wea. Rev.,* **137,** 2105–2125, doi:10.1175/2009MWR2645.1.

——, ——, J. F. Gamache, and F. D. Marks, 2011: Performance of convection-permitting hurricane initialization and prediction during 2008–2010 with ensemble data assimilation of inner-core airborne Doppler radar observations. *Geophys. Res. Lett.,* **38,** L15810, doi:10.1029/2011GL048469.

Zhao, Q., and Y. Jin, 2008: High-resolution radar data assimilation for Hurricane Isabel (2003) at landfall. *Bull. Amer. Meteor. Soc.,* **89,** 1355–1372, doi:10.1175/2008BAMS2562.1.

Zhu, K., Y. Pan, M. Xue, X. Wang, J. S. Whitaker, S. G. Benjamin, S. S. Weygandt, and M. Hu, 2013: A regional GSI-based ensemble Kalman filter data assimilation system for the Rapid Refresh configuration: Testing at reduced resolution. *Mon. Wea. Rev.,* **141,** 4118–4139, doi:10.1175/MWR-D-13-00039.1.